

TOPLESS promotes plant immunity by repressing auxin signaling and is targeted by the fungal effector Naked1

Fernando Navarrete¹, Michelle Gallei^{1,3}, Aleksandra E. Kornienko¹, Indira Saado², Mamoon Khan^{2,5}, Khong-Sam Chia², Martin A. Darino¹, Janos Bindics^{1,4} and Armin Djamei^{1,2,5,*}

¹Gregor Mendel Institute (GMI), Austrian Academy of Sciences (OeAW), Vienna BioCenter (VBC), Dr. Bohr-Gasse 3, 1030 Vienna, Austria

²Leibniz Institute of Plant Genetics and Crop Plant Research (IPK), OT Gatersleben, Corrensstraße 3, 06466 Stadt Seeland, Germany

³Present address: Institute of Science and Technology Austria, Am Campus 1, 3400 Klosterneuburg, Austria

⁴Present address: Institute of Molecular Biotechnology, Dr. Bohr-Gasse 3, 1030 Vienna, Austria

⁵Present address: Institute of Crop Science and Resource Conservation, University of Bonn, Bonn, Germany

*Correspondence: Armin Djamei (adjamei@uni-bonn.de)

<https://doi.org/10.1016/j.xplc.2021.100269>

ABSTRACT

In plants, the antagonism between growth and defense is hardwired by hormonal signaling. The perception of pathogen-associated molecular patterns (PAMPs) from invading microorganisms inhibits auxin signaling and plant growth. Conversely, pathogens manipulate auxin signaling to promote disease, but how this hormone inhibits immunity is not fully understood. *Ustilago maydis* is a maize pathogen that induces auxin signaling in its host. We characterized a *U. maydis* effector protein, Naked1 (Nkd1), that is translocated into the host nucleus. Through its native ethylene-responsive element binding factor-associated amphiphilic repression (EAR) motif, Nkd1 binds to the transcriptional co-repressors TOPLESS/TOPLESS-related (TPL/TPRs) and prevents the recruitment of a transcriptional repressor involved in hormonal signaling, leading to the de-repression of auxin and jasmonate signaling and thereby promoting susceptibility to (hemi)biotrophic pathogens. A moderate upregulation of auxin signaling inhibits the PAMP-triggered reactive oxygen species (ROS) burst, an early defense response. Thus, our findings establish a clear mechanism for auxin-induced pathogen susceptibility. Engineered Nkd1 variants with increased expression or increased EAR-mediated TPL/TPR binding trigger typical salicylic-acid-mediated defense reactions, leading to pathogen resistance. This implies that moderate binding of Nkd1 to TPL is a result of a balancing evolutionary selection process to enable TPL manipulation while avoiding host recognition.

Key words: topless, auxin, pattern-triggered immunity, PTI, effector, maize, *Ustilago maydis*

Navarrete F., Gallei M., Kornienko A.E., Saado I., Khan M., Chia K.-S., Darino M.A., Bindics J., and Djamei A. (2022). TOPLESS promotes plant immunity by repressing auxin signaling and is targeted by the fungal effector Naked1. *Plant Comm.* **3**, 100269.

INTRODUCTION

As sessile organisms, plants must integrate different endogenous and environmental signals to regulate growth and developmental programs. They have a limited set of resources that can be allocated to either growth or defense, and pathogen attack usually leads to decreased growth and fitness. Thus, pathogen attack constitutes a fundamental factor that negatively influences plant growth and yield in agricultural systems (Bethany et al., 2014).

Plants sense the presence of invading microbes through a series of plasma membrane receptors called pattern-recognition recep-

tors (PRRs) (Dangl and Jones, 2006; Dodds and Rathjen, 2010). PRRs recognize highly conserved microbial molecules such as bacterial flagellin or fungal chitin. These molecules are collectively referred to as pathogen-/microbial-associated molecular patterns (PAMPs/MAMPs). PRRs can also recognize endogenous molecules termed damage-associated molecular patterns (DAMPs) that are produced only after mechanical

Published by the Plant Communications Shanghai Editorial Office in association with Cell Press, an imprint of Elsevier Inc., on behalf of CSPB and CEMPS, CAS.

damage or pathogen invasion (Boller and Felix, 2009). Regardless of their origin, the recognition of PAMPs/DAMPs triggers a series of stereotypic responses collectively termed pattern-triggered immunity (PTI). These include an increase in cytosolic Ca^{2+} levels, production of reactive oxygen species (ROS) by plasma-membrane-localized nicotinamide adenine dinucleotide phosphate oxidase (NADPH oxidase), activation of mitogen-activated protein kinases (MAPKs), and transcriptional reprogramming, leading to growth inhibition (Dangl and Jones, 2006). PTI contributes to the inhibition of microbial colonization and must therefore be suppressed by pathogen-secreted molecules, effectors, to establish the interaction. Effectors are thus vital for disease progression. Depending on the host genotype, effectors can be recognized by resistance (R) proteins, which frequently belong to the nucleotide-binding, leucine-rich-repeat (NLR) class. This recognition, termed effector-triggered immunity (ETI), triggers a massive defense response and is often characterized by a form of apoptotic cell death, the hypersensitive response (HR) (Dangl and Jones, 2006; Boller and Felix, 2009). PTI and ETI do not act as independent immune systems, as they share many components. Moreover, it has recently been shown that PTI and ETI potentiate each other. ETI acts by increasing the expression levels of PRRs and NADPH oxidases, as it requires PAMP-triggered phosphorylation of PTI signaling components to achieve resistance, and PTI boosts ETI, as PAMPs enhance the HR (Ngou et al., 2021; Yuan et al., 2021).

Because the activation of defense responses is costly, it must be tightly regulated in order to optimize the trade-offs between growth and defense (Belkhadir et al., 2014; Bethany et al., 2014). Hormonal crosstalk plays a major role in regulating this process, and auxin, a growth-regulating hormone, has long been implicated in defense suppression. Despite being a well-studied phenomenon, the mechanisms of auxin-induced disease susceptibility toward biotrophs and hemi-biotrophs (pathogens that start as biotrophs but turn into necrotrophs during their life cycle) are not fully understood. Many pathogens produce auxins to promote disease, and exogenous auxin application has the same effect (Navarro et al., 2006; Ding et al., 2008; Suzuki et al., 2003; McClerkin et al., 2018). Auxin is thought to promote susceptibility in both salicylic acid (SA)-dependent and -independent manners. Auxin treatment can prevent SA-dependent production of pathogenesis-related proteins (PRs), which contribute to disease resistance (Aliab et al., 2018). This crosstalk is exploited by pathogenic bacteria. Besides synthesizing auxin, *P. syringae* uses the effector AvrRpt2 to target AUX/IAA repressor proteins, leading to increased auxin sensitivity and the suppression of SA-dependent defenses (Chen et al., 2007; Cui et al., 2013). The oomycete *Phytophthora parasitica* also exploits this phenomenon by secreting the effector PSE1, which modulates local auxin levels through the redistribution of the PIN-FORMED auxin transporters (Evangelisti et al., 2013). Auxin can also promote pathogen susceptibility independently of SA-mediated defenses, but the mechanism is unknown (Mutka et al., 2013). On the other hand, plants suppress auxin signaling following microbial recognition. Flagellin perception triggers the production of microRNA 393, which targets the auxin receptor TIR1, leading to the repression of auxin signaling and increased resistance to *P. syringae* (Navarro et al., 2006). Flagellin also triggers upregulation of *ICS1* and, subsequently, SA production (Tsuda et al., 2008).

Auxin is perceived largely in the nucleus. In their resting state, AUX/IAA repressors bind auxin response factors (ARFs) and repress their transcription by recruiting the TOPLESS and TOPLESS-related co-repressors (TPL/TPRs). TPL/TPRs are thought to act by recruiting histone deacetylases, therefore bringing the chromatin to a repressive state (Long et al., 2006; Szemenyei et al., 2008). In the presence of auxin, AUX/IAAs bind to TIR1/AFB receptors and are quickly ubiquitinated and degraded, subsequently releasing the repression of auxin-responsive genes (Mockaitis and Estelle, 2008).

TPL/TPRs mediate the repression of other hormonal and developmental pathways in addition to that of auxin, most notably those of jasmonate, brassinosteroids, and abscisic acid, which can also promote pathogen susceptibility (Pauwels et al., 2010; Causier et al., 2012; Oh et al., 2014; Lynch et al., 2017). Transcriptional repressors like AUX/IAAs use the short ethylene-responsive element binding factor-associated amphiphilic repression (EAR) motif to recruit TPL/TPRs. EAR motifs, together with the amino acid sequence LxLxL, mediate interaction with the N-terminal TOPLESS-related domain (TRD) of TPL/TPRs (Ke et al., 2015; Martin-Arevalillo et al., 2017). In addition, it has been shown that the interaction between *Arabidopsis thaliana* TPR1 and the R protein SNC1 is necessary for the activation of immune responses, although it seems to be independent of the presence of an EAR motif in SNC1 (Zhu et al., 2010).

Ustilago maydis is a fungal pathogen of maize. Infected plants form galls (cell masses derived from hypertrophy and hyperplasia) soon after infection, and these later become filled with fungal spores. Infected plants show an early transient upregulation and then suppression of genes involved in PTI, as well as an elevated expression of auxin-, jasmonate-, and gibberellin-responsive genes (Doehlemann et al., 2008). Galls have elevated auxin levels (Turian and Hamilton, 1960). Although *U. maydis* can synthesize auxin, the deletion of the necessary biosynthetic genes reduces auxin accumulation in galls but does not impair virulence (Reinecke et al., 2008). Thus, other factors, probably effector proteins, play a critical role in gall formation and virulence in this pathosystem. Effector-encoding genes tend to form in clusters in the *U. maydis* genome, and their deletion can lead to significant reductions in virulence (Kämper et al., 2006; Schirawski et al., 2010; Navarrete et al., 2021).

By contrast, SA is known to mediate resistance against *U. maydis*. The fungus secretes the translocated effector Cmu1, which reduces the amounts of precursors available for SA biosynthesis (Djamei et al., 2011). Another effector, Pit2, inhibits the activity of host cysteine proteases that mediate a positive feedback loop for the amplification of SA signaling in the apoplast (Ziemann et al., 2018). On the plant side, a recent report highlights the importance of SA and PTI for resistance to *U. maydis*. Maize *accelerated cell death 6* (*Zmacd6*) knockouts are more susceptible to *U. maydis* (Zhang et al., 2019). In *A. thaliana*, *ACD6* functions in SA-dependent immunity in the plasma membrane, where it interacts with several PRRs and promotes PAMP-triggered ROS bursts (Lu et al., 2003; Tateda et al., 2014), and *ZmACD6* can complement the susceptible phenotype of the *A. thaliana* knockout (Zhang et al., 2019).

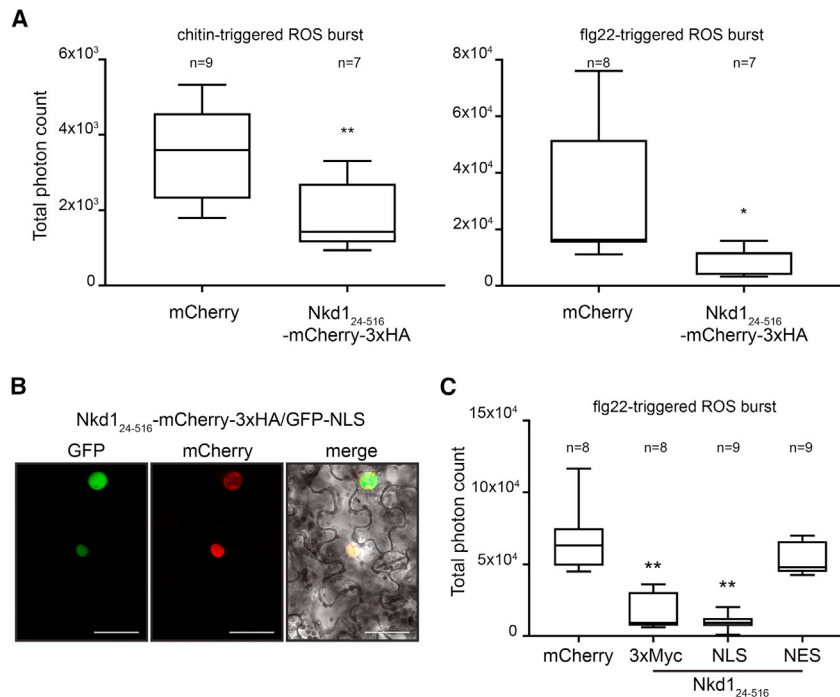


Figure 1. Nkd1 inhibits PAMP-triggered ROS bursts in the plant nucleus.

(A) PAMP-triggered ROS bursts in *N. benthamiana*. The effect of transient expression of Nkd1₂₄₋₅₁₆-mCherry-3xHA on ROS bursts triggered by chitin (left) or flg22 (right). Plants expressing mCherry were used as the positive control. Total photon counts indicating plant-derived apoplastic ROS were collected over 30 (chitin) or 40 (flg22) min and are depicted as boxplots. Data are a pool of three independent experiments (**p* < 0.05, ***p* < 0.01, *t* test).

(B) Localization of Nkd1 in *N. benthamiana*. Nkd1₂₄₋₅₁₆-mCherry-3xHA was co-expressed with GFP-NLS in epidermal cells, and localization was assessed by confocal microscopy. Nkd1₂₄₋₅₁₆-mCherry-3xHA localizes to the nucleus. Left panel: GFP fluorescence; middle panel: mCherry fluorescence; and right panel: bright field-GFP-mCherry merge. Scale bar, 50 μ m.

(C) Subcellular localization of Nkd1 affects ROS burst-suppressive activity. Nkd1₂₄₋₅₁₆-NLS retains its ability to suppress flg22-triggered ROS bursts, whereas Nkd1₂₄₋₅₁₆-NES does not. Data are a pool of three independent experiments (**p* < 0.05, ***p* < 0.01, ANOVA, Tukey's). For all panels, *n* = number of plants used for each group.

Here, we characterize a *U. maydis* effector found during a PTI inhibition screen. The protein, Naked1 (Nkd1), contains a functional EAR motif that mediates its interactions with members of the TOPLESS family of transcriptional co-repressors. Nkd1 is a virulence factor that acts in the maize nucleus. Nkd1 upregulates jasmonate and auxin signaling, and the latter leads to suppression of PAMP-triggered ROS bursts and increased pathogen susceptibility. We engineered variants of Nkd1 with altered affinity for members of the TOPLESS family and showed that increased binding to TPL/TPRs leads to resistance reactions, probably because of elevated SA signaling. Using Nkd1 as a tool, our experiments support the notion that TPL/TPRs are conserved molecular nodes in plant growth-defense antagonism signaling.

RESULTS

Nkd1 localizes to the nucleus and inhibits PAMP-triggered ROS bursts

We identified Nkd1 (UMAG_02299) during a PTI inhibition screen of candidate effector proteins from *U. maydis*. We expressed the protein in *Nicotiana benthamiana* by Agrobacterium-mediated transformation and tested its ability to suppress the PAMP-triggered ROS burst. Leaves expressing Nkd1₂₄₋₅₁₆-mCherry-3xHA (lacking the predicted secretion signal) or mCherry (positive control) were challenged with chitin or flg22, and ROS production was monitored over time. Plants expressing Nkd1₂₄₋₅₁₆-mCherry-3xHA showed a strongly reduced ROS burst compared with the mCherry control, regardless of the PAMP used (Figure 1A). Next, we verified the localization of Nkd1 in *N. benthamiana* by confocal microscopy. Plants co-expressing Nkd1₂₄₋₅₁₆-mCherry-3xHA and a GFP-nuclear localization signal (NLS; nuclear marker) showed that the effector protein localized exclusively to the nucleus (Figure 1B). We could not identify the presence of a strong NLS signal in the effector protein, and we therefore verified whether the nuclear localization of Nkd1 was

necessary for its immunity-suppressing activity using a mis-localization approach. We fused Nkd1 to either 3xMyc, an NLS, or a nuclear export signal (NES), expressed the fusion proteins in *N. benthamiana*, and measured PAMP-triggered ROS bursts. 3xMyc was used as a control because the Myc tag is not expected to alter protein localization. Plants expressing either Nkd1₂₄₋₅₁₆-3xMyc or Nkd1₂₄₋₅₁₆-NLS showed a markedly reduced ROS burst compared with the mCherry controls, whereas plants expressing Nkd1₂₄₋₅₁₆-NES did not (Figure 1C). We confirmed the localization of the fusion proteins in *N. benthamiana* by confocal microscopy using Nkd1₂₄₋₅₁₆-mCherry-3xHA, Nkd1₂₄₋₅₁₆-mCherry-NLS, and Nkd1₂₄₋₅₁₆-mCherry-NES (Supplemental Figure 1A). Effector fusions to mCherry-3xHA or mCherry-NLS showed a reduced ROS burst compared with the controls, whereas the mCherry-NES fusion did not (Supplemental Figure 1B). Therefore, our data indicate that the nuclear localization of Nkd1 in plant cells is necessary for immunity suppression.

Nkd1 promotes *U. maydis* virulence by targeting the maize nucleus

Because Nkd1 was originally found during a screen for putative effectors, we next asked whether it showed the characteristics of an effector protein. *nkd1* is located on chromosome five in the previously identified effector cluster 5–21 (Schirawski et al., 2010) (Supplemental Figure 2A). Analysis of *nkd1* expression by qPCR showed that it was induced in maize seedlings 1 day post-infection (dpi) and peaked between 6 and 8 dpi (Supplemental Figure 2B). Analysis of Nkd1 with SignalP 5.0 (Almagro Armenteros et al., 2019) predicted that amino acids 1 through 23 were a secretion signal. We therefore verified Nkd1 secretion by confocal microscopy during *U. maydis* infection in maize. We overexpressed the full-length Nkd1 fused to mCherry-3xHA (driven by the strong, biotrophy-specific *pit2* promoter [Lanver et al., 2018; Doehlemann et al., 2011]) and found that it localized

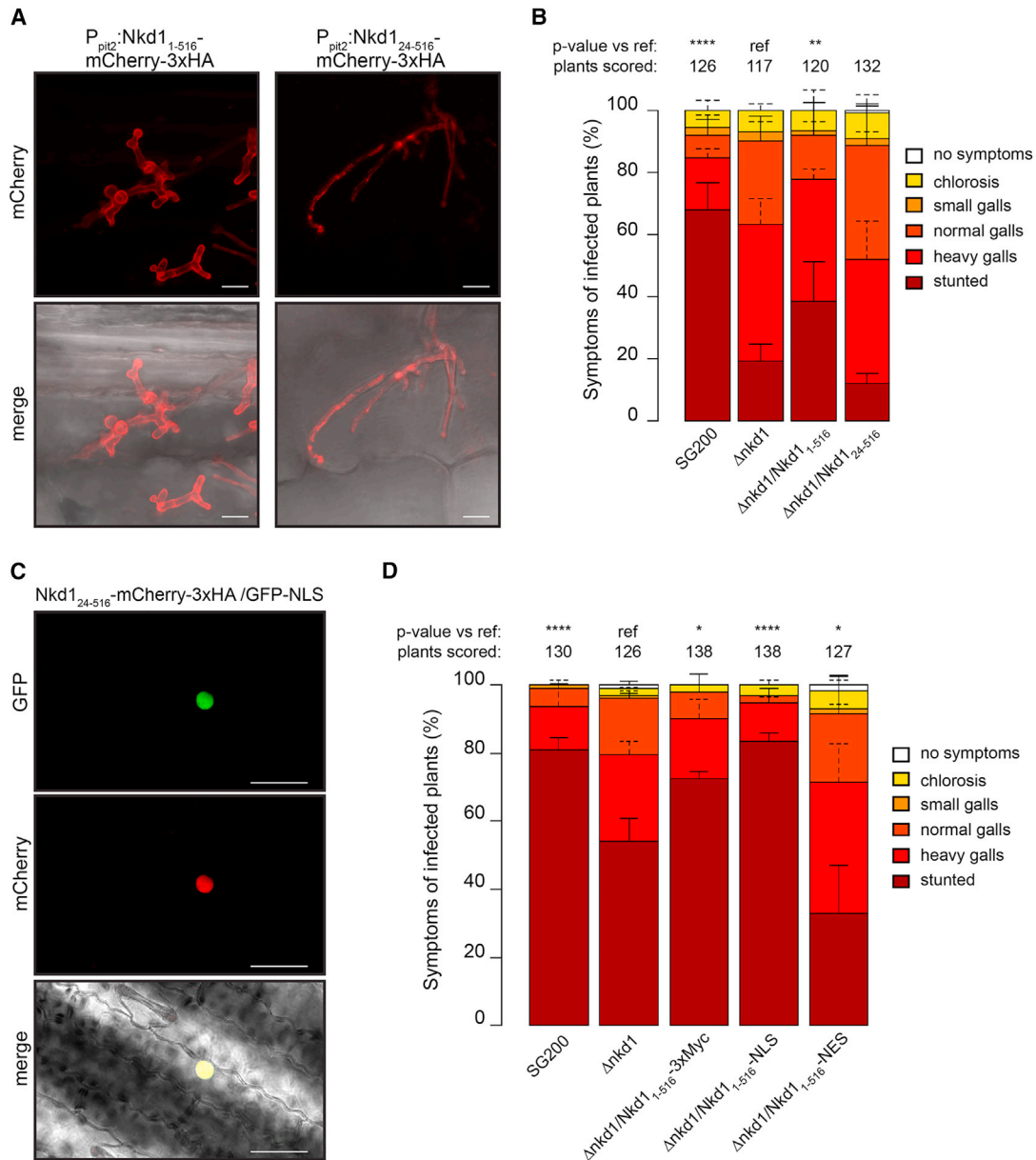


Figure 2. Nkd1 is a secreted protein that targets the host nucleus.

(A) Secretion of Nkd1 during maize infection. Left: *U. maydis* strain expressing $P_{pit2}::Nkd1_{1-516}$ -mCherry-3xHA shows mCherry signal at the periphery of the hyphae and hyphal tips. Right: *U. maydis* strain expressing $P_{pit2}::Nkd1_{24-516}$ -mCherry-3xHA (without its secretion signal) shows mCherry signal inside the hyphae. Pictures were taken 7 days post-infection (dpi) of maize seedlings. Upper panels: mCherry fluorescence; lower panels: bright-field-mCherry merge. Scale bar, 10 μ m.

(B) Disease symptom scoring of maize seedlings infected with *U. maydis* (7 dpi). SG200 (progenitor strain), $\Delta nkd1$, and two different complementation strains, either with ($Nkd1_{1-516}$) or without ($Nkd1_{24-516}$) the native secretion signal.

(C) Subcellular localization of Nkd1 in maize epidermal cells. $Nkd1_{24-516}$ -mCherry-3xHA was co-expressed with GFP-NLS in maize epidermal cells by biolistic bombardment. $Nkd1_{24-516}$ -mCherry-3xHA localizes to the nucleus. Upper panel: mCherry fluorescence; middle panel: GFP fluorescence; and bottom panel: bright-field-GFP-mCherry merge. Scale bar, 50 μ m.

(D) Disease symptom scoring of maize seedlings infected with *U. maydis* (7 dpi). SG200 (progenitor strain), $\Delta nkd1$, and Nkd1 fused to tags that affect its localization, 3xMyc (neutral), NLS (nucleus), and NES (cytoplasm). For (B) and (D), data represent mean \pm SD from three independent experiments; n = total number of scored plants. Significant differences between strains were analyzed by Fisher's exact test with a Benjamini-Hochberg correction for multiple comparisons (* $p < 0.05$, ** $p < 0.01$, *** $p < 0.001$, **** $p < 0.0001$).

to the edges and tips of the hyphae, indicating secretion (Figure 2A). We then plasmolyzed infected maize leaves, expanding the apoplastic space, and verified that Nkd1-mCherry-3xHA was freely diffusible in the apoplast

(Supplemental Figure 2C). By contrast, $Nkd1_{24-516}$ -mCherry-3xHA (lacking the predicted secretion signal) localized to the interior of the hyphae (Figure 2A) and was not detected in the maize apoplast (Supplemental Figure 2C), indicating that Nkd1

secretion depends on the presence of the predicted secretion signal. In addition, we also verified the secretion of Nkd1 in axenic culture. We used strain AB33, which filaments *in vitro*, mimicking some developmental changes undergone by *U. maydis* during host colonization (Brachmann et al., 2001). We detected Nkd1₁₋₅₁₆-3xHA in both pellet and supernatant fractions, indicating that the protein was released from the hyphae, whereas the non-secreted actin control was detected only in the pellet fraction (Supplemental Figure 2D).

We then generated deletion strains in the solopathogenic SG200 *U. maydis* background and infected maize seedlings to test whether *nkd1* contributes to virulence. Plants infected with the $\Delta nkd1$ strain showed milder symptoms than the SG200-infected plants. Stunting symptoms were noticeably reduced in $\Delta nkd1$ -infected plants (Figures 2B and Supplemental Figure 2E). Next, we tested whether the secretion of Nkd1 contributes to virulence. We ectopically complemented the $\Delta nkd1$ mutant with constructs encoding the full-length protein (Nkd1₁₋₅₁₆) or its derivative without the predicted secretion signal (Nkd1₂₄₋₅₁₆) and infected maize seedlings. Nkd1₁₋₅₁₆ was able to partially complement the virulence defect of the $\Delta nkd1$ mutant, but Nkd1₂₄₋₅₁₆ was not, indicating that Nkd1 secretion is necessary for virulence (Figure 2B).

Because we had shown earlier that nuclear localization of Nkd1 in *N. benthamiana* cells was required for the inhibition of defenses, we verified the subcellular localization of Nkd1 in maize cells. We co-expressed 35S:Nkd1₂₄₋₅₁₆-mCherry-3xHA with 35S:GFP-NLS in maize epidermal cells by biolistic bombardment. Confocal microscopy showed that Nkd1₂₄₋₅₁₆-mCherry-3xHA co-localized with GFP-NLS in the maize nucleus and that no mCherry signal could be detected in the cytoplasm (Figure 2C). We then tested whether localization to the maize nucleus was necessary for the virulence function of Nkd1. We used a mis-localization approach identical to that used for ROS burst suppression in *N. benthamiana*. We generated $\Delta nkd1$ complementation strains expressing full-length Nkd1 fused to either 3xMyc, NLS, or NES. Expression of Nkd1₁₋₅₁₆-3xMyc or Nkd1₁₋₅₁₆-NLS complemented the virulence defect of the $\Delta nkd1$ mutant, whereas expression of Nkd1₁₋₅₁₆-NES did not (Figure 2D). This result indicated that localization to the host nucleus is required for Nkd1 function. The fusion of Nkd1₁₋₅₁₆ to mCherry-3xHA was not able to rescue the virulence defect of the $\Delta nkd1$ mutant (Supplemental Figure 2F), despite the fact that Nkd1₂₄₋₅₁₆-mCherry-3xHA was active in plant cells (Supplemental Figure 1). Because fusion to large, structurally stable proteins like GFP or mCherry has been reported to inhibit effector translocation but not secretion in *U. maydis* (Tanaka et al., 2015), we interpret this result as further confirmation that Nkd1 is translocated into host cells.

Taken together, our results from *N. benthamiana* and maize infection experiments indicate that Nkd1 is secreted from *U. maydis* and translocated into the host nucleus, where it promotes virulence. Furthermore, our data also imply that the target(s) of Nkd1 are conserved between monocots and dicots.

Nkd1 binds to TPL/TPRs to suppress the PAMP-triggered ROS burst

To gain further insight into the function of Nkd1, we performed homology searches using BLAST. We found homologs of UmNkd1

only in the closely related smut fungi *Pseudozyma hubeiensis*, *Sporisorium reilianum*, *S. scitamineum*, *S. graminicola*, and *Melanopsichium pennsylvanicum*. A close examination of the C-terminal sequences of these proteins revealed the presence of an LxLxL-type EAR motif that was conserved across most of the orthologs. In *S. scitamineum*, the second L residue is substituted with the structurally related I, and in *M. pennsylvanicum* (which shows the lowest overall sequence homology to UmNkd1), the motif is missing completely (Figure 3A). We therefore evaluated whether the presence of an EAR motif was important for the function of the Nkd1 orthologs. We expressed UmNkd1, SrNkd1, SsNkd1, and MpNkd1 without their predicted secretion signals in *N. benthamiana* and tested their ability to suppress immunity as before. All orthologs were expressed as full-length proteins and localized to the nucleus (Supplemental Figure 3A and 3B), but only MpNkd1, which lacks the EAR motif, failed to suppress the PAMP-triggered ROS burst (Figure 3B). This result indicates that the EAR motif may be required for this process.

Because the EAR motif is known to mediate protein interactions with TPL/TPRs in plants (Causier et al., 2012), these results prompted us to investigate whether UmNkd1 interacts with members of the TPL/TPR family. We constructed *U. maydis* strains expressing UmNkd1-3xHA or mCherry-3xHA driven by the *Umpit2* promoter, which confers strong expression during biotrophic development (Doehlemann et al., 2011; Lanver et al., 2018), and we used these strains to infect maize seedlings. We extracted total proteins from infected tissues and immunoprecipitated hemagglutinin (HA)-tagged proteins with α -HA magnetic beads. By western blotting with α -TPL antibodies, we showed co-immunoprecipitation (coIP) of TPL proteins with UmNkd1-3xHA but not with mCherry-3xHA (Figure 3C), indicating that the TPLs interacted with the effector protein. To confirm this interaction, we co-expressed ZmTPL1-3xMyc and NbTPR3-3xMyc with UmNkd1₂₄₋₅₁₆-3xHA or YFP-3xHA in *N. benthamiana* and immunoprecipitated TPL/TPRs with α -Myc magnetic beads. UmNkd1₂₄₋₅₁₆-3xHA, but not YFP-3xHA, co-immunoprecipitated with ZmTPL1-3xMyc and NbTPR3-3xMyc, confirming our previous results (Figure 3D). We next performed a yeast two-hybrid (Y2H) assay to test whether the interaction between UmNkd1 and TPL/TPRs was direct. TPL/TPR homologs from maize and *A. thaliana* were fused with the GAL4BD and used to test their interaction with UmNkd1₂₄₋₅₁₆ or mCherry fused with the GAL4AD. UmNkd1 interacted with all homologs tested, with the exception of ZmTPL2, and it seemed to show a preference for ZmTPL1/ZmTPL4 and AtTPR2/AtTPL/AtTPL1, as evidenced by differential growth on different selective media (Figure 3E). This apparent preference for certain homologs may indicate sub-specialization of the different TPL/TPRs, but this possibility requires further study. Because we had earlier shown the importance of plant nuclear targeting for Nkd1 activity, we verified that the interaction between Nkd1 and TPL/TPRs occurs in this subcellular compartment by a split-Venus assay (Gookin and Assmann, 2014). Indeed, we detected a fluorescent signal in the nucleus when ZmTPL1-CVenus was co-expressed with Nkd1-NVenus fusions but not when ZmTPL1-CVenus was co-expressed with the negative control NLS-luciferase-NVenus, even though all proteins used in the assay were expressed at similar levels (Figure 3F). These results indicated that the interaction of Nkd1 with TPL/TPRs occurs in the plant nucleus.

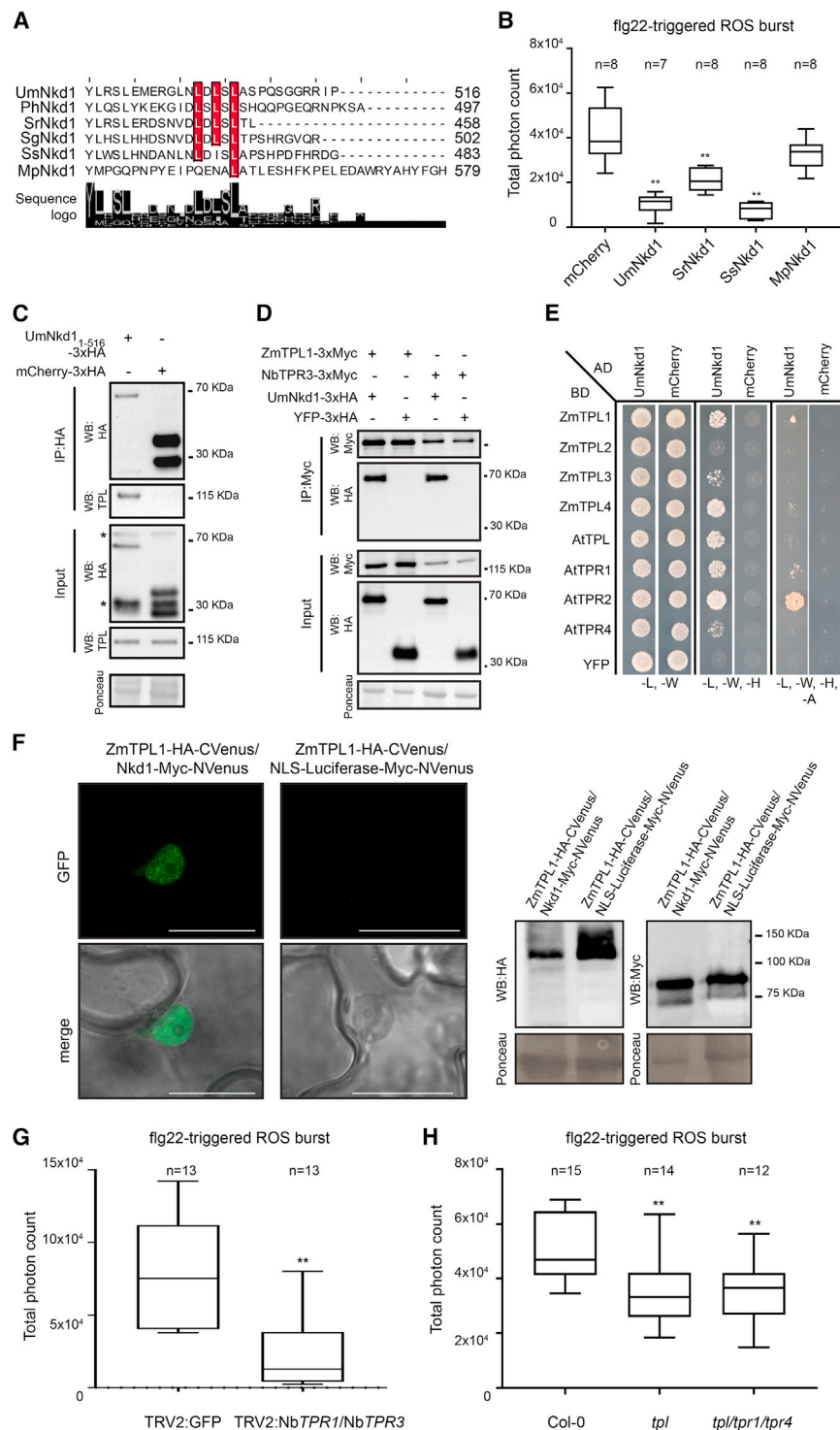


Figure 3. Nkd1 interacts with members of the TOPLESS family.

(A) Protein alignment of the C-terminal portion of Nkd1 and its orthologs (Um: *U. maydis*; Ph: *Pseudozyma hubensis*; Sr: *Sporisorium reilianum*; Sg: *Sporisorium graminicola*; Ss: *Sporisorium scitami-neum*; Mp: *Melanopsichium pennsylvanicum*). Conserved leucine residues corresponding to the EAR motif are highlighted in red. Numbers on the right indicate protein length in (A).

(B) PAMP-triggered ROS burst suppression in *N. benthamiana* expressing different Nkd1 orthologs (without their predicted secretion signals). Only MpNkd1, which lacks the EAR motif, is unable to suppress the PAMP-triggered ROS burst. Plants expressing mCherry were used as the positive controls. Total photon counts over 40 min are shown as boxplots. Data are a pool of three independent experiments (** $p < 0.01$, ANOVA, Tukey's).

(C) UmNkd1 interacts with TPL during maize infection. Maize plants were infected with a *U. maydis* strain carrying P_{PHI2}:Nkd1₁₋₅₁₆-3xHA or P_{PHI2}:Nkd1₁₋₂₃-mCherry-3xHA. Total proteins were immunoprecipitated with α -HA magnetic beads (IP: HA) and blotted with specific antibodies. ZmTPLs co-immunoprecipitate with Nkd1₁₋₅₁₆-3xHA but not with mCherry-3xHA. *, nonspecific band.

(D) UmNkd1 interacts with members of the TPL family in *N. benthamiana*. Total proteins were immunoprecipitated with α -Myc magnetic beads (IP: Myc) and blotted with specific antibodies. UmNkd1₂₄₋₅₁₆-3xHA, but not YFP-3xHA, co-immunoprecipitates with ZmTPL1-3xMyc and NbTPR3-3xMyc.

(E) Y2H assay showing interaction of UmNkd1₂₄₋₅₁₆ with TPL homologs. Yeast strains were grown on SD media lacking the indicated amino acids/nucleotides. Growth in medium lacking leu (L) and trp (W) was used as the transformation control. Growth in intermediate-stringency medium lacking leu (L), trp (W), and his (H) or high-stringency medium lacking leu (L), trp (W), his (H), and ade (A) indicated protein interaction.

(F) Left panels: split-Venus assay showing the interaction of Nkd1-Myc-NVenus and ZmTPL1-HA-CVenus (fluorescent signal) in the nucleus of *N. benthamiana* epidermal cells. Co-expression of NLS-luciferase-Myc-NVenus with ZmTPL1-HA-CVenus does not lead to a fluorescent signal in the plant nuclei. Scale bar, 20 μ m. Right panels: western blot showing the expression of all proteins used in the assay.

(G) flg22-triggered ROS bursts in *N. benthamiana* plants in which *TPR1* and *TPR3* were silenced by VIGS. TRV2:GFP was used as an off-target control.

(H) flg22-triggered ROS bursts in *A. thaliana* Col-0 and *tpl* mutants.

For (G) and (H), total photon counts over 40 min are shown as boxplots. Data are a pool of three independent experiments (** $p < 0.01$, Tukey's ANOVA). For all panels, n = number of plants used for each group.

The interaction between UmNkd1 and TPL/TPRs suggested that these plant proteins were involved in PTI, a function not previously attributed to them. We therefore tested this hypothesis by

silencing *TPRs* in *N. benthamiana* by virus-induced gene silencing and assessing *tpl/tpr* mutants in *A. thaliana*. NbTPR1/TPR3-silenced plants and single (*tpl*) or triple (*tpl/tpr1/tpr4*)

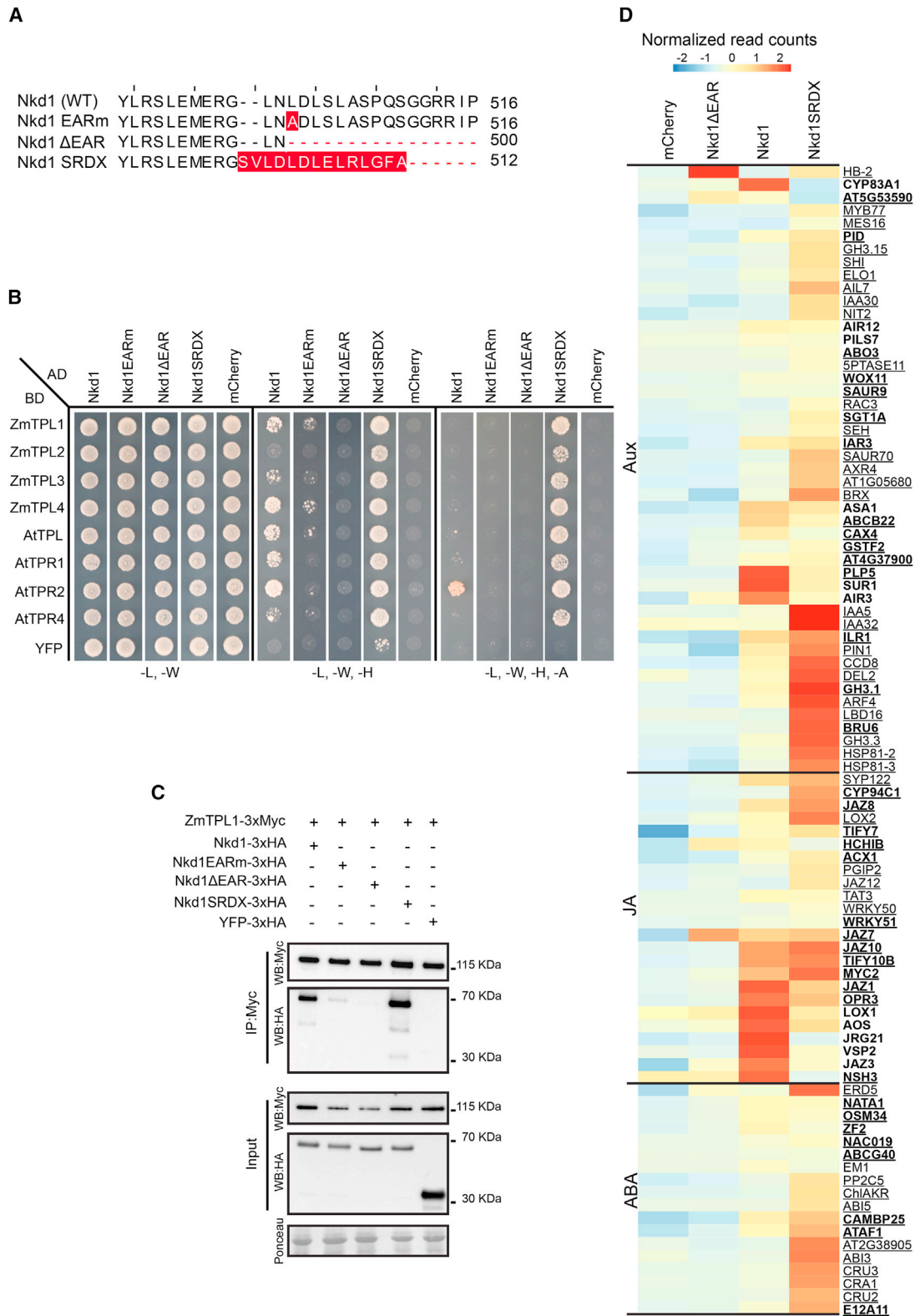


Figure 4. The EAR motif of Nkd1 mediates binding to TPL/TPRs and de-repression of hormone signaling.

(A) Protein alignment of the C-terminal portion of UmNkd1 and its EAR mutants. For each protein, the mutated residues are highlighted in red. Numbers on the right indicate the protein length in aa.

(legend continued on next page)

A. thaliana knockout plants showed a reduced PAMP-triggered ROS burst compared with their controls (Figures 3G and 3H). Therefore, taken together, our data suggest that TPL/TPRs regulate PAMP-triggered ROS bursts and that Nkd1 proteins target TPL/TPRs to suppress this process.

The EAR motif of Nkd1 mediates its binding to TPL/TPRs and the de-repression of hormonal signaling

Because we had shown previously that MpNkd1 (which lacks an EAR motif) could not suppress immunity, we mutated the EAR motif in UmNkd1 and evaluated its effect on binding to TPL/TPRs. Three mutants were produced: Nkd1EARm (L501A, alanine substitution in the first position of the conserved EAR motif), Nkd1ΔEAR (deletion of the last 16 amino acids, including the EAR motif), and Ndk1SRDX (Nkd1ΔEAR fused to SRDX, an optimized EAR motif derived from the SUPERMAN transcription factor) (Hiratsu et al., 2003) (Figure 4A). Using Y2H assays, we showed that Nkd1EARm had reduced binding to TPL/TPRs from maize and *A. thaliana*. Only minor growth was visible on intermediate stringency medium (-L, -W, -H) compared with the wild-type (WT) control. Nkd1ΔEAR did not bind to any of the TPL/TPRs, as indicated by a lack of growth on the intermediate stringency medium. By contrast, Ndk1SRDX showed an increased binding to TPL/TPRs compared with the WT control, as indicated by strong growth on both the intermediate and high stringency media (-L, -W, -H, -A). In addition, this mutant was the only one that showed an interaction with ZmTPL2 (Figure 4B). We then confirmed these results by coIP in *N. benthamiana*. We co-expressed ZmTPL1-3xMyc with either Nkd1-3xHA, Nkd1EARm-3xHA, Nkd1ΔEAR-3xHA, Ndk1SRDX-3xHA, or YFP-3xHA and immunoprecipitated total proteins with α-Myc magnetic beads. Nkd1EARm-3xHA and Nkd1ΔEAR-3xHA showed strongly reduced binding to ZmTPL1-3xMyc compared with the WT control, as indicated by the strongly reduced or absent signal in the α-HA blot of the immunoprecipitated (IP) fraction (Figure 4C). On the other hand, Ndk1SRDX-3xHA co-precipitated with ZmTPL1-3xMyc and showed stronger binding than that of the WT control, as indicated by the increased signal in the α-HA blot of the IP fraction (Figure 4C). Our results thus indicate that Nkd1 interacts with TPL/TPRs through its EAR motif and that the specific sequence of this motif determines the strength of the interaction.

Because TPL/TPRs are such important regulators of transcription, we aimed to assess the effects of Nkd1 on plant gene expression. Taking advantage of the fact that UmNkd1 binds to TPL/TPRs from different species, we generated transgenic *A. thaliana* plants expressing the effector protein under the control of an estradiol-

inducible promoter. *A. thaliana* seedlings expressing either Nkd1-3xMyc, Nkd1ΔEAR-3xMyc, Nkd1SRDX-3xMyc, or mCherry-3xMyc (reference control) were treated with estradiol for 5 and 24 h, and gene expression was monitored by RNA sequencing (RNA-seq). We observed transcriptomic changes that varied according to the strength of the interaction between the different Nkd1 variants and the TPL/TPRs. The number of differentially expressed genes (DEGs) was higher in plants expressing Nkd1SRDX-3xMyc than in plants expressing Nkd1-3xMyc and Nkd1ΔEAR-3xMyc (Supplemental Figure 4, Figure 4D; Supplemental Table 1). For instance, 5 h after estradiol treatment, we detected 2,156, 910, and 21 upregulated genes in Nkd1SRDX-3xMyc-, Nkd1-3xMyc-, and Nkd1ΔEAR-3xMyc-expressing plants, respectively (Supplemental Figure 4A). Because the latter plants showed so few DEGs, this indicates that most, if not all, physiological changes induced by the expression of Nkd1 in *A. thaliana* derive from EAR-mediated interactions with plant proteins. Also, plants expressing Nkd1SRDX-3xMyc showed a different pattern of DEGs. At both time points, only about 50% of the DEGs were upregulated, whereas in Nkd1-3xMyc plants, this fraction included approximately 90% of the DEGs (Supplemental Figure 4A).

Gene Ontology (GO) term analysis of DEGs identified 5 h after estradiol treatment showed that most upregulated genes belonged to the classes “defense response,” “response to other organism,” and “immune response.” The enrichment of these categories was several orders of magnitude higher in plants expressing Nkd1SRDX-3xMyc than in plants expressing Nkd1-3xMyc (Supplemental Figure 4B). These categories contain many of the genes involved in PTI responses such as *RLKs*, *MAPKs*, and the plasma membrane NADPH oxidase *RBOHD*, which is responsible for the PAMP-triggered ROS burst, and therefore indicate that immunity suppression by Nkd1 is most likely post-transcriptional.

We then examined other GO categories (with fewer DEGs) that could explain the susceptibility toward biotrophs. These included “response to endogenous stimulus,” “cellular response to jasmonic acid stimulus,” “cellular response to hypoxia,” and “response to hormone.” These pathways contain genes whose transcriptional regulation is mediated by TPL/TPRs and that rely on transcriptional repressors with EAR motifs of the same type as that found in Nkd1 (Szemenyei et al., 2008; Pauwels et al., 2010; Causier et al., 2012; Lynch et al., 2017). Lines expressing Nkd1-3xMyc and Nkd1SRDX-3xMyc showed an overlapping but slightly different set of upregulated genes involved in the signaling and metabolism of auxin and jasmonic acids. We observed the upregulation of typical early auxin-responsive genes

(B) Y2H assay showing interaction of Nkd1 and its EAR mutants with TPL homologs. Yeast strains were grown on SD media lacking the indicated amino acids/nucleotides. Growth in medium lacking leu (L) and trp (W) was used as the transformation control. Growth in intermediate-stringency medium lacking leu (L), trp (W), and his (H) or high-stringency medium lacking leu (L), trp (W), his (H), and ade (A) indicated protein interaction.

(C) Interaction of Nkd1 and its EAR mutants with ZmTPL1 *in planta*. Total proteins were immunoprecipitated from *N. benthamiana* with α-Myc magnetic beads (IP: Myc) and blotted with specific antibodies. Nkd1-EARm and Nkd1ΔEAR show a reduced affinity for ZmTPL1, whereas Nkd1SRDX shows an increased affinity for ZmTPL1.

(D) Heatmap showing the expression levels of hormone-responsive genes in *A. thaliana* seedlings 5 h post-induction of transgene expression. Aux, auxin; JA, jasmonic acid; ABA, abscisic acid; responsive/homeostatic genes. Genes depicted here are differentially expressed in at least one of the lines compared with the mCherry-expressing plants (controls). Bold: significantly misregulated in Nkd1. Underlined: significantly misregulated in Nkd1SRDX. Data are the average of three independent experiments. Differential gene expression was analyzed with DESeq2 using a threshold of log2 fold change > 0.6, and *p* < 0.01 (Benjamini-Hochberg correction).

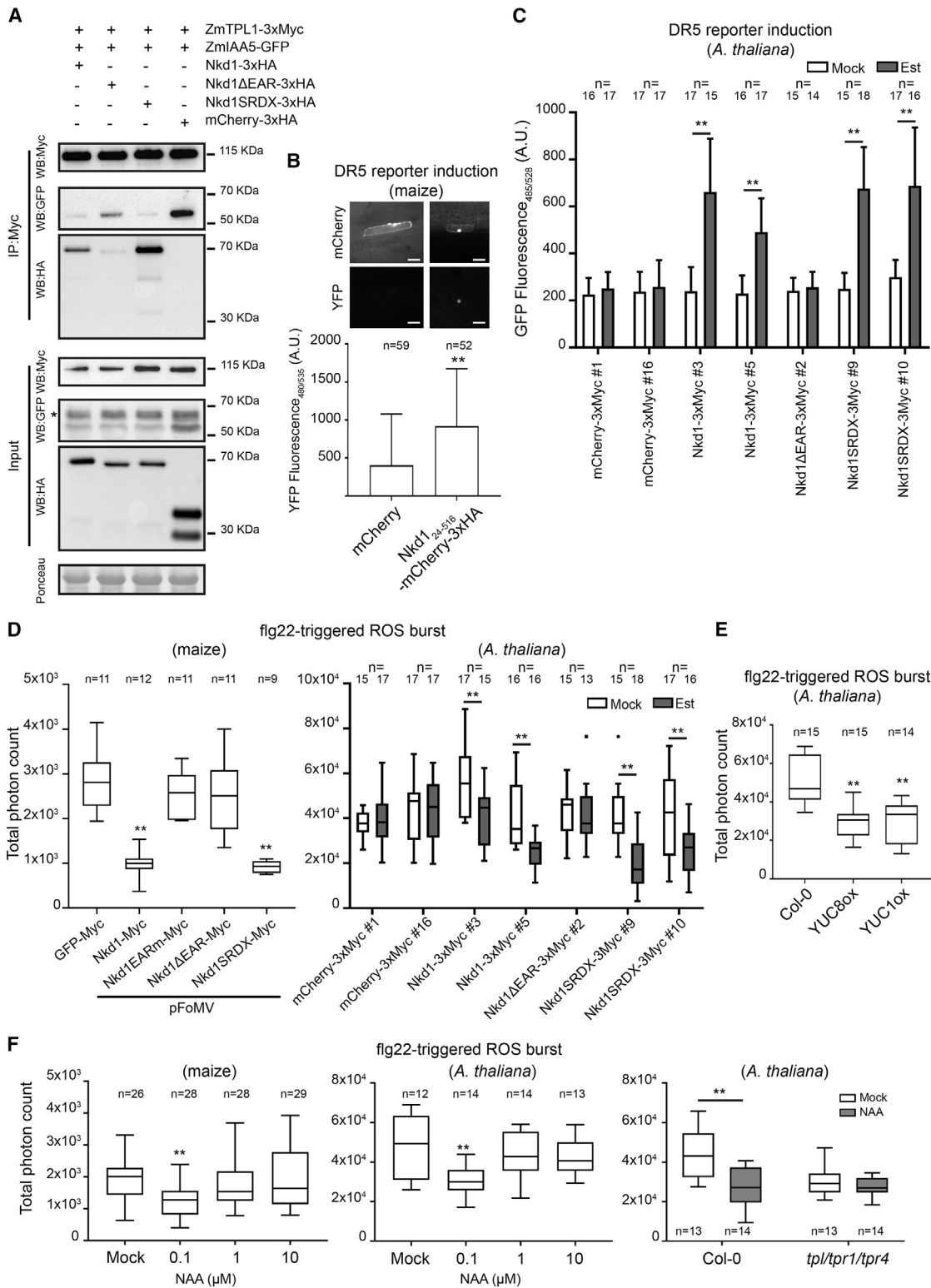


Figure 5. TPL/TPR mediated repression of auxin signaling is required for PAMP-triggered ROS bursts.

(A) Proteins were immunoprecipitated from *N. benthamiana* with α -Myc magnetic beads (IP: Myc) and blotted with specific antibodies. ZmIAA5 co-precipitates with ZmTPL1 in the presence of Nkd1ΔEAR or mCherry but not in the presence of Nkd1 or Nkd1SRDX. *, nonspecific band. (B) Nkd1₂₄₋₅₁₆-mCherry-3xHA or mCherry were co-expressed with DR5:YFP in maize epidermal cells. Top: representative pictures of cells expressing either mCherry or Nkd1₂₄₋₅₁₆-mCherry-3xHA. Scale bar, 50 μ m. Bottom: reporter activity quantified by fluorescence intensity (528 nm) of transformed cells. Data are a pool of three independent experiments; mean \pm SD (***p* < 0.01, *t* test).

(legend continued on next page)

such as *GH3.1*, *BRU6*, and *SAUR9* in plants expressing either Nkd1-3xMyc or Nkd1SRDX-3xMyc, but the latter also showed upregulation of *GH3.3*, *LBD16*, and *AUX/IAA* repressors and the *PIN1* auxin transporter (Figure 4D; Supplemental Table 1). Plants expressing either Nkd1-3xMyc or Nkd1SRDX-3xMyc also showed upregulation of typical early jasmonic-acid-responsive genes, such as biosynthetic genes and *JAZ* transcriptional repressors, although different *JAZ* homologs were induced in the two lines (Figure 4D; Supplemental Table 1). In addition, plants expressing Nkd1SRDX-3xMyc showed stronger upregulation of abscisic-acid-responsive genes compared with plants expressing Nkd1 (Figure 4D; Supplemental Table 1).

Overall, our results indicate that the specific sequence of the EAR motif of Nkd1 determines the strength of its interaction with TPL/TPRs, the degree to which the latter can repress gene expression, and, in consequence, the plant responses to the different Nkd1 variants.

TPL/TPR-mediated repression of auxin signaling is required for PAMP-triggered ROS burst

Because our previous data suggested that the EAR-mediated interaction between Nkd1 and TPL/TPRs leads to the upregulation of TPL/TPR repressed genes (Figure 4), we hypothesized that Nkd1 can affect the recruitment of TPL/TPRs to transcriptional repressors that contain EAR motifs. We tested this hypothesis by assessing the ability of AUX/IAA proteins to bind to TPL/TPRs in the presence of Nkd1. We co-expressed ZmTPL1-3xMyc and ZmIAA5-GFP in the presence of either Nkd1-3xHA, Nkd1ΔEAR-3xHA, Nkd1SRDX-3xHA, or mCherry-3xHA in *N. benthamiana* and immunoprecipitated ZmTPL1 with α-Myc magnetic beads. ZmIAA5-GFP was able to co-precipitate with ZmTPL1-3xMyc in the presence of mCherry-3xHA or Nkd1ΔEAR-3xHA but not in the presence of Nkd1-3xHA or Nkd1SRDX-3xHA (Figure 5A), indicating that the EAR-motif-mediated binding of Nkd1 to TPL/TPRs prevents their recruitment to AUX/IAA5 and probably mediates the upregulation of hormone-responsive genes. To confirm this result, we co-expressed 35S:Nkd1₂₄₋₅₁₆-mCherry-3xHA or 35S:mCherry with the DR5:YFP auxin reporter in maize epidermal cells by biolistic bombardment. Nkd1-mCherry-3xHA was able to upregulate the expression of the DR5:YFP reporter compared with the mCherry control (Figure 5B). Furthermore, Nkd1-3xMyc and Nkd1SRDX-3xMyc, but not Nkd1EARm-3xMyc or Nkd1ΔEAR-3xMyc, were able to upregulate the expression of the DR5:GFP reporter in *A. thaliana* and *N. benthamiana* (Figures 5C and Supplemental Figure 5C). In addition, UmNkd1, SrNkd1, and SsNkd1, but not

MpNkd1 (which lacks an EAR motif), were able to upregulate the expression of the DR5 reporter upon transient expression in *N. benthamiana* (Supplemental Figure 5D).

We also evaluated the effect of the EAR mutations on the ability of Nkd1 to suppress the PAMP-triggered ROS burst. We transiently expressed different Nkd1 variants in maize using vectors derived from the Foxtail mosaic virus (pFoMV) (Bouton et al., 2018). Consistent with our observations of the DR5 reporter, Nkd1 and Nkd1SRDX, but not Nkd1EARm or Nkd1ΔEAR, were able to suppress PAMP-triggered ROS bursts in maize plants compared with the GFP control (Figure 5D). This occurred despite the fact that constructs encoding different Nkd1 variants produced uneven viral loads and thus different protein amounts in maize (Supplemental Figure 5A and 5B). We confirmed this result by expressing the same effector variants in *A. thaliana* and *N. benthamiana* (Figure 5D and Supplemental Figure 5E). The effect of the EAR mutations on Nkd1-mediated inhibition of PAMP-triggered ROS bursts was independent of the PAMP used, as the same phenotypes were observed when plants were treated with chitin or elf18 (Supplemental Figure 5F and 5G). Our results thus indicate either that Nkd1 affects auxin signaling and PAMP-triggered ROS simultaneously or that the upregulation of auxin signaling can suppress PAMP-triggered ROS bursts.

To test this hypothesis, we assessed PTI in *YUC8*- and *YUC1*-overexpressing *A. thaliana* lines (which have high endogenous auxin levels) (Zhao et al., 2001; Hentrich et al., 2013). Both lines showed a reduced PAMP-triggered ROS burst compared with the WT Col-0 background (Figure 5G). In addition, we tested the effect of elevated auxin signaling on PAMP-triggered ROS bursts by overexpressing different ARFs in *N. benthamiana*. We chose ZmARF18 and ZmARF2 because they are upregulated during maize infection by *U. maydis* (Doehlemann et al., 2008). ZmARF18 is an activator from the AtARF6/8 class, whereas ZmARF2 is a repressor from the AtARF6/10/17 class (Xing et al., 2011). The expression of WT or microRNA-resistant versions of ZmARF18 was enough to inhibit the flg22-triggered ROS burst, but expression of WT or microRNA-resistant ZmARF2 had no effect. AtARF5 and NbARF5 (also activator ARFs) did not affect flg22-triggered ROS bursts, possibly because of their very low expression levels (Supplemental Figure 5H and 5I). We also treated maize and *A. thaliana* plants with the auxin analog naphthaleneacetic acid (NAA). At 100 nM, but not at higher concentrations, NAA led to a reduction in flg22-triggered ROS bursts in both plant species (Figure 5F). Finally, we evaluated the effect of *tpl* mutations on auxin-mediated ROS burst

(C) Nkd1 and Nkd1SRDX, but not Nkd1ΔEAR, upregulate the expression of the DR5:GFP reporter in *A. thaliana*. Data are a pool of three independent experiments; mean ± SD (***p* < 0.01, Tukey's ANOVA).

(D) Left panel: Nkd1 variants were expressed transiently in maize with the pFoMV viral vector. Nkd1 and Nkd1SRDX, but not Nkd1EARm or Nkd1ΔEAR, inhibit flg22-triggered ROS bursts at 9 dpi. Data (total photon counts over 20 min) are a pool of three independent experiments (***p* < 0.01, Tukey's ANOVA). Right panel: Nkd1 and Nkd1SRDX, but not Nkd1ΔEAR, inhibit PAMP-triggered ROS bursts in *A. thaliana*. Data (total photon counts over 40 min) are a pool of three independent experiments (***p* < 0.01, Bonferroni's two-way ANOVA).

(E) *A. thaliana* plants overexpressing YUCCA proteins have reduced flg22-triggered ROS bursts compared with Col-0. Data (total photon counts over 40 min) are a pool of three independent experiments (***p* < 0.01, left/center: Tukey's ANOVA).

(F) Auxin inhibits flg22-triggered ROS bursts. Maize (left) and *A. thaliana* (center) plants treated with 0.1 μM NAA show reduced ROS bursts compared with the mock treatment. Right: treatment of *A. thaliana* with 0.1 μM NAA inhibits the ROS burst in the WT but not in the *tpl1/tp1/tp4* triple mutant. Data (total photon counts over 40 min) are a pool of 4 (left) or 3 (center and right) independent experiments (***p* < 0.01, left/center: Tukey's ANOVA, right: Bonferroni's two-way ANOVA). For all panels, n = number of samples used for each group.

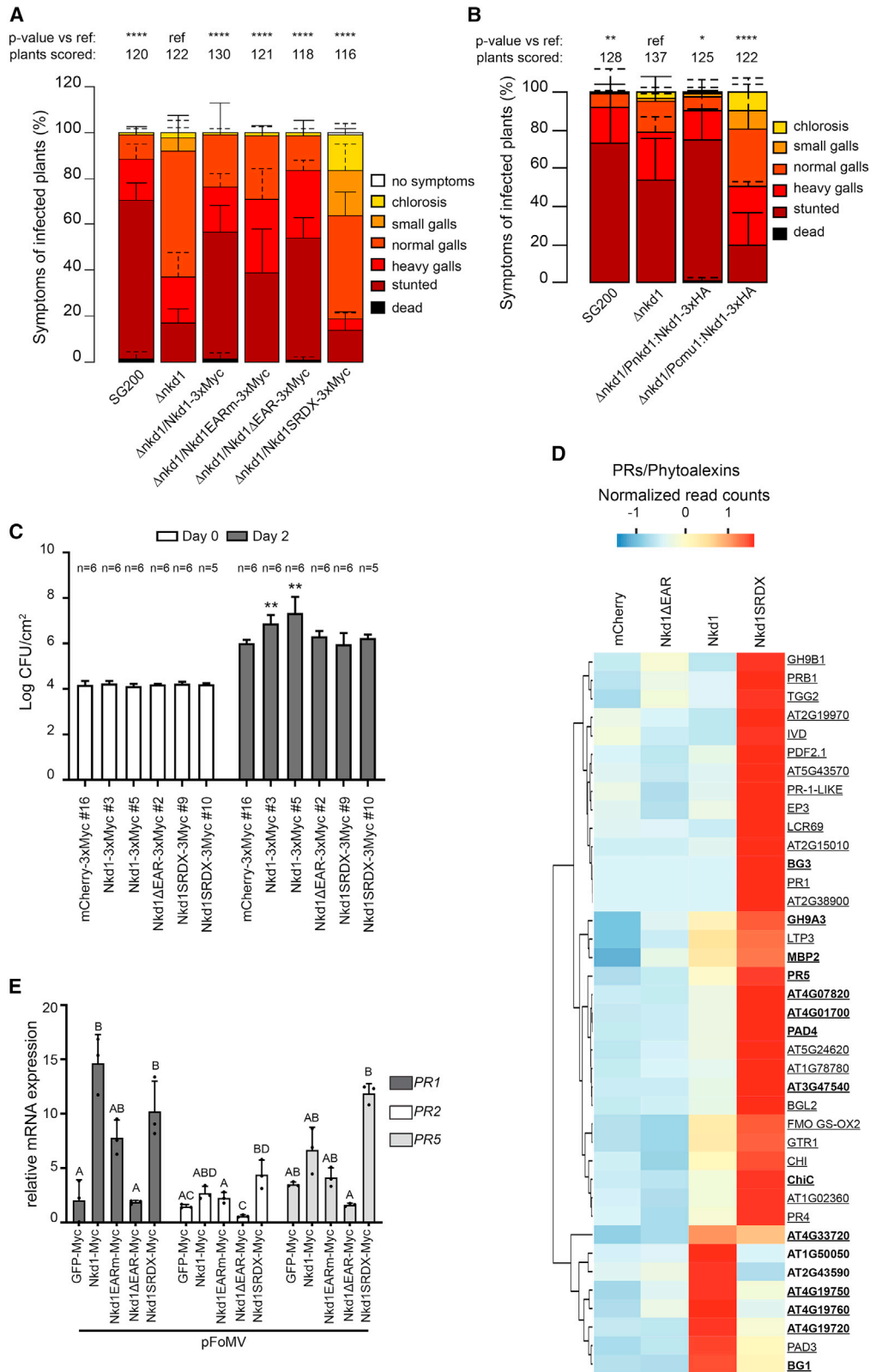


Figure 6. The EAR motif of Nkd1 affects host susceptibility to pathogens.

(A) Disease symptom scoring of maize seedlings infected with *U. maydis* SG200 (progenitor strain), Δ nkd1, and different complementation strains carrying mutations in the EAR motif (7 dpi). Nkd1 (WT), Nkd1EARm, and Nkd1 Δ EAR are able to complement the virulence defect of *U. maydis* Δ nkd1, but Nkd1SRDX is not. Data represent mean \pm SD from three independent experiments, and n = total number of scored plants. Significant differences between

(legend continued on next page)

inhibition. NAA treatment led to a reduced flg22-triggered ROS burst in Col-0 but not in the *tpl1/tpr1/tpr4* knockout mutant (Figure 5F), indicating that TPL/TPRs are necessary for auxin-mediated suppression of the PAMP-triggered ROS burst.

Overall, our results indicate that the binding of Nkd1 to TPL/TPRs prevents the recruitment of ZmAUX/IAA5, and possibly other transcriptional repressors, leading to an upregulation of auxin signaling and subsequent suppression of the PAMP-triggered ROS burst.

Increased Nkd1 binding to TPL/TPRs triggers resistance reactions

To evaluate how the binding of Nkd1 to TPL/TPRs affects the virulence of *U. maydis*, we ectopically complemented the $\Delta nkd1$ mutant with constructs encoding the WT protein or its EAR mutants (Nkd1EARm, Nkd1 Δ EAR, and Nkd1SRDX). Remarkably, Nkd1EARm and Nkd1 Δ EAR complemented the virulence defect of the $\Delta nkd1$ mutant, similar to the levels observed with WT *nkd1*. Even more unexpectedly, complementing $\Delta nkd1$ with Nkd1SRDX led to an even more pronounced virulence defect than that observed in the knockout (Figure 6A). A similar phenotype was observed when the expression of *nkd1* was dramatically increased during infection in maize. Complementation of $\Delta nkd1$ with P_{Cmu1}:*nkd1* (the *cmu1* promoter shows very high expression during infection; Djamei et al., 2011) also led to a more pronounced virulence defect than that observed in the knockout (Figure 6B). We then used propidium iodide, which stains cells with compromised plasma membranes and cell walls, to assess host cell viability during infection with the different strains (Doehlemann et al., 2009; Jones et al., 2016). Maize plants infected with either $\Delta nkd1$ /P_{Nkd1}:*nkd1*-SRDX or $\Delta nkd1$ /P_{Cmu1}:*nkd1* showed death of the cells surrounding the invading hyphae, whereas this was not observed in plants infected with SG200, $\Delta nkd1$, or $\Delta nkd1$ /*nkd1* (Supplemental Figure 6). This result indicates that the pronounced virulence defect of the former two strains is due to increased cell death/immune reactions.

To gain insight into how plants react to Nkd1 beyond the suppression of PAMP-triggered ROS bursts, we infected *A. thaliana* lines expressing Nkd1 or its EAR mutants with *Pseudomonas syringae* pv. tomato DC3000 (Pst) and evaluated the subsequent bacterial colonization. Expression of WT Nkd1 led to an increased suscep-

tibility to Pst. These lines showed a 6- to 30-fold increase in bacterial populations compared with plants expressing mCherry (the reference control). By contrast, bacterial counts in plants expressing Nkd1 Δ EAR or Nkd1SRDX did not differ from those in plants expressing mCherry (Figure 6C). Taking all experiments together, the fact that Nkd1EARm and Nkd1 Δ EAR complement the virulence defect of the $\Delta nkd1$ mutant but do not promote susceptibility of *A. thaliana* to Pst indicates that *U. maydis* uses other effectors to target TPL/TPRs in addition to Nkd1. Furthermore, the contribution of Nkd1 to the virulence of *U. maydis* probably depends on interactions with targets other than the TPL/TPRs. On the other hand, the fact that Nkd1SRDX is not able to complement the $\Delta nkd1$ mutant or to promote susceptibility of *A. thaliana* to Pst indicates that “mild” binding to TPL/TPRs (as seen for WT Nkd1) promotes pathogen susceptibility, whereas increased binding strength/specificity (as seen for Nkd1SRDX or by dramatically increasing *nkd1* expression using the *cmu1* promoter) triggers resistance reactions, independent of the suppression of PAMP-triggered ROS bursts.

To assess the factors that could explain the lack of susceptibility to Pst in *A. thaliana* plants expressing Nkd1SRDX, we searched our RNA-seq data for genes that were differentially expressed between these plants and plants expressing WT Nkd1. Clustering analysis indicated that plants expressing Nkd1SRDX formed a unique group, different from those expressing Nkd1, 24 h after induction of transgene expression (Supplemental Figure 7A). We therefore focused on this time point. Among the most variable DEGs in this group, we found enrichment of PRs, R genes, and genes involved in phytoalexin synthesis or metabolism (Figures 6D and Supplemental Figure 7B; Supplemental Tables 2 and 3), which are typical SA-mediated responses (Robert-Seilaniantz et al., 2011). PR expression, in particular, was one to three orders of magnitude higher in plants expressing Nkd1SRDX than in plants expressing Nkd1 (WT) (Supplemental Table 2). In addition, we observed cell-death symptoms 3 days after induction of transgene expression in adult *A. thaliana* plants expressing Nkd1 and Nkd1SRDX. The symptoms were stronger in lines expressing Nkd1SRDX, and these plants did not recover 1 week after the treatment. Plants expressing Nkd1 Δ EAR or mCherry did not show any cell-death symptoms (Supplemental Figure 8A). In *N. benthamiana*, cell-death

strains were analyzed by Fisher's exact test with a Benjamini-Hochberg correction for multiple comparisons (* $p < 0.05$, ** $p < 0.01$, *** $p < 0.001$, **** $p < 0.0001$).

(B) Disease symptom scoring of maize seedlings infected with *U. maydis* SG200 (progenitor strain), $\Delta nkd1$, and $\Delta nkd1$ complemented with *nkd1* driven by the native promoter or by a strong biotrophy-specific promoter from *cmu1* (7 dpi). Use of the *cmu1* promoter to drive expression of *nkd1* exacerbates the virulence defect of the $\Delta nkd1$ strain.

For (A) and (B), data represent mean \pm SD from three independent experiments; n = total number of scored plants. Significant differences between strains were analyzed by Fisher's exact test with a Benjamini-Hochberg correction for multiple comparisons (* $p < 0.05$, ** $p < 0.01$, *** $p < 0.001$, **** $p < 0.0001$).

(C) Bacterial growth in *A. thaliana* expressing different Nkd1 constructs. Plants expressing mCherry were used as the control. Nkd1 (WT) promotes susceptibility of *A. thaliana* to *P. syringae*, but Nkd1 Δ EAR and Nkd1SRDX do not. Data are one representative experiment from a total of three; n = number of plants used for each group. Significant differences between lines were analyzed by Tukey's ANOVA (** $p < 0.01$).

(D) Heatmap showing the expression levels of PRs and phytoalexin biosynthetic and regulatory genes in *A. thaliana* seedlings 24 h post-induction of transgene expression (Euclidian clustering). Genes depicted are differentially expressed in at least one of the lines compared with the mCherry-expressing plants (controls). Bold: significantly upregulated in Nkd1. Underlined: significantly upregulated in Nkd1SRDX. Data are the average of three independent experiments. Genes significantly upregulated in both Nkd1 and Nkd1SRDX lines are highlighted in bold. Differentially expressed genes were identified with DESeq2 using a threshold of log₂ fold change > 0.6, and $p < 0.01$ (Benjamini-Hochberg correction).

(E) PR gene expression in maize plants expressing the respective viral constructs was monitored by qRT-PCR and normalized to that of *ZmCDK* at 9 dpi. Data are mean \pm SD; n = 3 (different letters indicate significant differences, $p < 0.01$, Tukey's ANOVA).

symptoms (observed 8 dpi) were not distinguishable between Nkd1 and Nkd1SRDX. The expression of Nkd1EARm led mainly to chlorosis, and there was minimal cell death near the infiltration point. The expression of Nkd1ΔEAR led to only very mild chlorosis and no cell death, nearly indistinguishable from the response of the mCherry control (Supplemental Figure 8B).

To verify whether these responses were also observed macroscopically in maize plants upon the expression of the different effector variants, we used the pFoMV vectors and assessed their effects on *PR* and *NLR/HR* gene expression. In general, Nkd1-expressing plants showed increased expression of *PRs* compared with Nkd1ΔEAR-expressing plants. In the case of *ZmPR2*, only plants expressing Nkd1SRDX showed an increased expression compared with GFP- (control) or Nkd1ΔEAR-expressing plants. For *ZmPR1* and *ZmPR5*, Nkd1SRDX-induced *PR* expression was not different from Nkd1 (WT)-induced *PR* expression, despite the fact that viral spread and effector protein accumulation were much lower in the former plants (Figure 6E, Supplemental Figure 5A and 5B).

Maize plants expressing Nkd1 and Nkd1SRDX showed mild cell-death symptoms (15 dpi), but these were not distinguishable from each other. Plants expressing either Nkd1EARm, Nkd1ΔEAR, or GFP did not show any cell-death symptoms (Supplemental Figure 8C). In addition, we did not observe an upregulation of *NLR* gene expression in maize plants expressing any of the effector variants compared with the GFP control (Supplemental Figure 7C).

Taken together, our results indicate that increased binding of Nkd1 to TPL/TPRs leads to a pronounced upregulation of SA-responsive genes, including *NLRs* and *PRs*, whose expression pattern seems to be more conserved between monocots and dicots. Together, they increase resistance toward biotrophic pathogens despite the reduction in PAMP-triggered ROS bursts.

DISCUSSION

Auxin has long been implicated in the suppression of plant defenses, as many pathogens produce this hormone and, in some cases, auxin biosynthetic genes are located in pathogenicity islands (Yamada, 1993). Other than the inhibition of SA-mediated defenses, it is not clear how elevated auxin levels or signaling can promote disease susceptibility. Here, we provide evidence that auxin signaling inhibits PAMP-triggered ROS bursts, one of the earliest plant defense responses induced after microbial perception, and that this mechanism is exploited by the fungal effector Nkd1. We have shown that Nkd1 is secreted from *U. maydis* and is translocated into the host nucleus, where it targets TPL/TPRs. EAR-motif-mediated binding of Nkd1 to TPL/TPRs prevents their recruitment to Aux/IAA5 and possibly other transcriptional repressors, leading to elevated auxin signaling and the subsequent inhibition of PTI. This inhibition is likely post-transcriptional, as we observed an upregulation of many PTI-related genes, including *NADPH* oxidases, in plants expressing Nkd1. Nkd1 probably also promotes host susceptibility through the upregulation of jasmonic acid signaling, a well-documented phenomenon (Robert-Seilaniantz et al., 2011; Jiang et al., 2013). Therefore, our data suggest that the upregulation of hormonal signaling induced by Nkd1 leads to

defense inhibition, although we do not exclude other effects such as involvement in gall development. Our results thus complement the previous observation that flg22 inhibits auxin signaling (Navarro et al., 2006; Navarro et al., 2004). They shed light on the mechanisms underlying the mutual antagonism between auxin signaling and PTI and suggest why many pathogens (including non-gall-inducing pathogens) manipulate host auxin signaling.

Previously, effector translocation into host cells was demonstrated using reporter strains or differential cultivar sets that rely on the HR to indicate the presence of an effector in the plant cytosol (Mudgett et al., 2000; Wang et al., 2017). None of these tools are available in the *U. maydis*-maize pathosystem, and effector translocation has therefore been demonstrated by technically demanding assays like immunolabeling followed by electron microscopy (Djamei et al., 2011; Redkar et al., 2015), functional read outs (Tanaka et al., 2014), or transgenic labeling approaches (Lo Presti et al., 2017). Here, we made use of the virulence defect of the $\Delta nkd1$ mutant and the strong nuclear localization of Nkd1₍₂₄₋₅₁₆₎ *in planta* to show that Nkd1 is a translocated protein. Restricting Nkd1 nuclear entry (by fusion to the NES signal) prevents complementation of the $\Delta nkd1$ virulence defect. This is consistent with the observations that Nkd1 is solely nuclear-localized when it is expressed in maize cells, it interacts with TPL/TPRs (nuclear proteins) in the native system during infection, and its expression in plants leads to decreased PAMP-triggered ROS bursts in an EAR-motif-dependent manner, phenocopying the *tpl* knockout. Our results are thus in line with previous observations showing that knockout of *TPL/TPRs* in *A. thaliana* leads to an increased susceptibility to *Pst*, whereas overexpression of *TPR1* increases resistance to this pathogen (Zhu et al., 2010; Niu et al., 2019).

Although WT Nkd1 inhibits PTI, this is unlikely to be the reason for the virulence defect observed in the $\Delta nkd1$ mutant. PTI-inhibiting effectors are highly redundant in *U. maydis*, as we have recently shown (Navarrete et al., 2021). We also identified another *U. maydis* effector, Jsi1, that targets TPL/TPRs. Jsi1 lacks any homology to Nkd1 but contains a DLNxxP-type EAR motif that mediates its interaction with one of the C-terminal WD40 domains of TPL/TPRs. The deletion of *jsi1* does not lead to virulence defects, and its expression *in planta* induces an overlapping but different set of hormone-responsive genes, predominantly from the jasmonate/ethylene branch (Darino et al., 2021). Therefore, the different domains of TPL/TPR proteins seem to control different hormone-responsive gene sets.

Despite the fact that Nkd1-mediated PTI inhibition depends on its interaction with TPL/TPRs via the EAR motif, complementation of the $\Delta nkd1$ mutant with constructs encoding Nkd1 versions that do not bind to TPL/TPRs restored virulence to near-WT levels. Because complementation of the $\Delta nkd1$ mutant depends on the nuclear localization of the protein in the host cell, this indicates that the $\Delta nkd1$ virulence defect is due to a second, as yet unknown, function of Nkd1 in the host cell nucleus. This scenario is feasible considering that Nkd1 is relatively large for an effector (65 kDa), but its ability to inhibit PTI depends on the very short C-terminal EAR motif, and that many effectors target several

unrelated host proteins (Xin et al., 2018; Park et al., 2012; Shi et al., 2018). In addition to a second, unidentified host target, another explanation for the virulence function of Nkd1 could be its interaction with one or more additional effectors that depend on Nkd1 to perform their function in maize. Systematic Y2H screens between *U. maydis* effectors indicate a massive effector interactome (Alcantara et al., 2019), and effector-effector interactions have been shown to impact virulence in other pathosystems (Tzfira et al., 2004; Cain et al., 2008; Magori and Citovsky, 2011). Although we could not detect an interaction between Nkd1 and Jsi1 (Alcantara et al., 2019), Nkd1 could potentially interact with other *U. maydis* effectors during maize infection. Therefore, analysis of Nkd1 interaction partners (plant or fungal) by IP-mass spectrometry (MS) of infected maize tissue could help to identify its second, non-redundant function.

Recent data suggest that TPL/TPRs may also be involved in SA signaling. NPR3 and NPR4 are negative regulators of this defense pathway that repress SA-responsive genes in the absence of an SA stimulus. Both NPR3/4 contain EAR motifs, and mutation of this motif abolishes the repressor activity of NPR4 (Ding et al., 2018). Furthermore, NPR3 has recently been shown to interact with TPL (Altmann et al., 2020). In addition, another set of negative regulators of SA signaling, the NIMINs, contain EAR motifs, and NIMIN1 has been shown to interact with TPL (Weigel et al., 2001; Consortium, 2011). However, the functional relevance of the interaction between these negative regulators of SA and TPL/TPRs has not been characterized to date. Thus, similar to the interaction between TPL/TPRs and AUX/IAAs observed here, it is feasible that Nkd1 and Nkd1SRDX may interfere with the interaction between TPL/TPRs and NIMINs or NPR3/4. However, the latter effector may do this to a greater extent, for example, by interfering with both NIMINs and NPR3/4, whereas Nkd1 (WT) may interfere with a single one of these systems. This possibility is consistent with the fact that upregulation of SA-responsive genes occurs upon the expression of both effectors, but Nkd1SRDX induces a far greater expression of SA-responsive genes like PRs and NLRs, and it does not induce pathogen susceptibility. In addition, Nkd1SRDX leads to a very marked reduction in *U. maydis* virulence and in the spread of FoMV in maize. This resistance response induced by Nkd1SRDX may involve the interaction between TPL/TPRs and R proteins. A recent report showed that the interaction between AtTPR1 and the R protein SNC1 leads to increased expression of R genes and growth inhibition (Cai et al., 2019), similar to our observations here in *A. thaliana*. In maize, we observed host cell death in tissues around the Nkd1SRDX-expressing invading hyphae but found no upregulation of NLRs. It may be that we simply did not find the NLRs involved in this process or that the cell-death symptoms observed in this plant do not require the upregulation of NLRs.

Nevertheless, there seems to be an optimum strength for the EAR-mediated Nkd1 interaction with TPL/TPRs. In WT Nkd1, the EAR motif mediates interaction with TPL/TPRs to upregulate auxin signaling and inhibit PAMP-triggered ROS bursts. However, if the binding strength is increased and/or the specificity for different TPL homologs is expanded (as in the case of Nkd1SRDX) or if the effector expression is increased to non-

physiological levels (*cmu1* promoter), additional defense responses are triggered that prevent pathogen susceptibility, despite the inhibition of PAMP-triggered ROS bursts.

In conclusion, we have identified a regulatory circuit in which a pathogen effector targets TPL/TPRs to upregulate auxin signaling and suppress PTI. Nonetheless, this immune suppression is not effective when other defense responses (mediated by *PR* and *R* genes) are triggered. This is in line with our experiments showing that NAA can inhibit PTI at a concentration optimum of 100 nM but not higher. It is also in line with previous observations (Navarro et al., 2006) that the auxin-mediated promotion of Pst susceptibility was not effective when R-gene-mediated responses were activated. Our finding that the EAR motif is conserved among most Nkd1 orthologs, as well as in other TPL-binding effectors in *U. maydis* and other pathogens (Gawehns, 2014; Petre et al., 2015; Darino et al., 2021), suggests that fungi widely exploit the antagonism between growth and defense by targeting the central co-repressor TOPLESS. The discovery of the post-transcriptional mechanism by which TOPLESS-dependent elevated auxin signaling inhibits PTI awaits further research.

MATERIALS AND METHODS

Protein sequence analysis

For candidate effector genes, sequences were screened for the presence of a secretion signal with SignalP 5.0 (Almagro Armenteros et al., 2019). Protein alignments and neighbor-joining phylogenetic trees were constructed in CLC Main Workbench 7.7.2.

Plasmids, cloning procedures, and generation of *U. maydis* strains

All plasmids were generated by standard molecular procedures (Sambrook et al., 2006). *E. coli* strain Mach1 (Thermo Fisher Scientific, Waltham, MA, USA) was used for all DNA manipulations. All other plasmids were generated by the GreenGate system (Lampropoulos et al., 2013). The modules used were either amplified by PCR or obtained from the published system. In addition, we generated two GreenGate destination vectors, pADGG and pBDGG, based on the pGAD and pGBKT7 backbones, respectively, that were used for Y2H assays. Plasmids used for virus-induced gene silencing (VIGS) assays in *N. benthamiana* were generated by Gateway Cloning (Katzen, 2007). For transient virus-mediated overexpression, PV101 (Bouton et al., 2018) was used to generate pFoMV:p19-P2A-mCherry-P2A-effector-Myc and pFoMV:p19-P2A-mCherry-P2A-GFP-Myc using the NotI-XbaI cloning sites (p19: silencing suppressor, P2A: viral ribosome skipping motif). Unless otherwise stated, effector proteins were expressed without their secretion signals.

U. maydis knockout strains were generated by homologous recombination with PCR-derived constructs (Kämper, 2004). For complementation and protein expression, strains were generated by the insertion of p123 derivatives into the *ip* locus (Loubradou et al., 2001). At least two independent strains were tested for each complementation construct. Transformants were verified by southern blotting or PCR. All plasmids and strains used in this study can be found in the [supplemental information](#).

Maize infection assays

Virulence assays and disease symptom scoring were performed as described by Kämper et al. (2006). In brief, *U. maydis* SG200 and its derivatives were cultured in liquid YepsLight (0.4% yeast extract, 0.4% peptone, and 2% sucrose) at 28°C to an OD_{600nm} of 0.6–0.8. Cells were

pelleted by centrifugation at $2400 \times g$ for 10 min and resuspended in H_2O to an OD_{600nm} of 1. The suspensions were then syringe-inoculated into seven-day-old B73 maize seedlings. Maize was grown in a temperature-controlled glasshouse (14 h light/10 h dark, $28^\circ C/20^\circ C$), and disease symptoms were assessed at 7 dpi. The filamentous growth of the *U. maydis* strains was tested by spotting the strains on CM agar (Brachmann et al., 2001) containing 1% activated charcoal. The experiments were repeated at least three times.

Viral-mediated protein expression and biolistic bombardment in maize

Biolistic bombardment was performed according to Djamei et al. (2011) with minor modifications. In brief, 1.6- μm gold particles were coated with plasmid DNA encoding the indicated constructs under the control of the CaMV35S promoter. Bombardment was performed on 7-day-old maize leaves cv. B73 using a PDS-1000/HeTM instrument (Bio-Rad) at 900 psi in a 27-Hg vacuum. Fluorescence was observed by confocal microscopy 18–24 h after bombardment. The experiments were repeated at least three times. Viral-mediated protein expression derived from the FoMV infectious clone has been described previously (Bouton et al., 2018). Plasmids were bombarded into whole seedlings, and plants were returned to the growth chamber.

Analysis of gene expression in maize by qRT-PCR

Samples were obtained nine days post-bombardment, and mCherry fluorescence was monitored as an indication of viral spread. Areas with positive mCherry fluorescence were used for RNA extraction. Total RNA was extracted with the RNeasy Plant Mini Kit according to the manufacturer's instructions (Qiagen, catalog [cat.] no. 74904). On-column DNase treatment was performed with the RNase-Free DNase Set (Qiagen, cat. no. 79254). One microgram of total RNA was used for cDNA synthesis with RevertAid Reverse Transcriptase (Thermo Fisher, cat. no. EP0442). qPCRs were performed with GoTaq qPCR mix (NEB, cat. no. A6001) according to the manufacturer's instructions using 0.5 μL of cDNA product. Relative amounts of amplicons were calculated according to the $2^{-\Delta\Delta Ct}$ method (Livak and Schmittgen, 2001) with *CDK* (GRMZM2G149286/Zm00001d010476) as a reference gene (Lin et al., 2014).

Cell death assessment in maize

Dead tissue was detected in whole maize leaves with trypan blue staining (Fernandez-Bautista et al., 2016). Leaves were completely immersed in a fresh trypan blue solution (containing 85% lactic acid, 99% glycerol, phenol, ddH_2O , and trypan blue). After 30 min, stained leaves were immediately washed in 98% ethanol and left in it overnight. The ethanol solution was then replaced until the green tissue was cleared.

Quantification of DR5 reporter activity in maize by epi-fluorescence microscopy

DR5:GFP was co-expressed with 35S:Nkd1-mCherry-3xHA or 35S:mCherry in maize leaves as described above, and GFP fluorescence (Ex 480/40 nm, Em 535/50 nm) was quantified from the double-transformed cells using a widefield microscope equipped with transmitted and fluorescent light sources (Axio Imager.Z2). In brief, the fluorescence intensity (535/50 nm) of each sample was calculated as the pixel intensity of the double-transformed cells minus the pixel intensity of the untransformed cells (background) using FIJI (Schindelin et al., 2012). At least 20 doubly transformed cells/treatment were analyzed per experiment. Experiments were repeated three times.

Confocal microscopy

Confocal microscopy was performed with a Zeiss LSM 700 or LSM 780 confocal microscope. GFP was excited at 488 nm using an argon laser. Fluorescence emission was collected between 500 and 540 nm. mCherry was excited at 561 nm, and emission was collected between 578 and 648 nm. Images were processed with ZEN 2.3 lite (blue edition). Fungal

proliferation in infected tissue was assessed at 5 dpi. Chitin was stained with wheat germ agglutinin (WGA) coupled with AlexaFluor488 (Invitrogen). Plant cell walls and membrane-compromised cells were stained with propidium iodide (Sigma-Aldrich, St. Louis, MO, USA). Leaf samples were incubated with 10 $\mu g/mL$ WGA-AF488 and 1 $\mu g/mL$ propidium iodide and were observed as described above. WGA-AF488 and propidium iodide excitation/detection conditions were as described for GFP and mCherry, respectively.

Protein secretion in *U. maydis*

For the visualization of secreted proteins in infected tissues, maize plants were harvested at 6–7 dpi and analyzed by confocal microscopy as described above. For plasmolysis experiments, infected maize tissue was infiltrated with 1 M mannitol and incubated at least 30 min prior to observation. Experiments were repeated at least three times.

Secreted proteins from fungal cultures were detected as previously described (Djamei et al., 2011). *U. maydis* was grown in Complete Medium (CM) medium to an OD_{600nm} of 0.6–0.8, centrifuged, resuspended in Ammonium Medium (AM) medium, and incubated for 5–6 h to induce filamentation. Cultures were centrifuged, and supernatant proteins were precipitated with 10% trichloroacetic acid and 0.02% sodium deoxycholate and resuspended in 100 mM Tris (pH 8). Proteins from the cell pellets were extracted by adding an SDS loading buffer and a spatula tip of glass beads and vortexing for 10 min. All extracts were subjected to immunoblotting using α -HA (Sigma-Aldrich, St. Louis, MO, USA) for detection of effector proteins and α -actin antibodies (Invitrogen, Waltham, MA, USA) for lysis control. Experiments were repeated two times.

Yeast transformation and two-hybrid assays

All yeast protocols were performed according to the Yeast Protocols Handbook (Clontech, Mountainview, CA, USA) with minor modifications. Strain AH109 was transformed with bait vectors (pGBKT7 and derivatives), and strain Y187 was transformed with prey vectors (pAD, pADGG, and derivatives) by the LiAc/PEG method. All positive clones were verified for the presence of the corresponding plasmid by DNA extraction with 20 mM NaOH and PCR (Supplemental information). For one-to-one matings, AH109 pBDGG-ZmTPL1, pBDGG-ZmTPL2, pBDGG-ZmTPL3, pBDGG-ZmTPL4, pBDGG-AtTPL, pBDGG-AtTPR1, AtTPR2, AtTPR4, or pBDGG-YFP were mated against Y187 pADGG-Nkd1, pADGG-Nkd1EARm, pADGG-Nkd1 Δ EAR, pADGG-Nkd1SRDX, or pADGG-mCherry. Diploid cells were selected on SD -leu, -trp medium. For plate drop out assays, diploid cells were grown in liquid SD -leu, -trp medium overnight. Cells were pelleted by centrifugation at $500 \times g$ for 3 min and resuspended in sterile H_2O to an OD_{600nm} of 1. Serial dilutions were made in H_2O , and 5 μL of the suspensions were plated in SD -leu, -trp (growth control), SD -leu, -trp -his (intermediate stringency), and SD -leu, -trp, -his, -ade (high stringency) media. Growth in intermediate or high stringency media at 4 dpi indicated positive interactions. Experiments were repeated three times.

Plant growth conditions and chemical treatments

N. benthamiana and *A. thaliana* plants were grown in controlled short-day conditions (8 h light/16 h dark, $21^\circ C$) in a soil:perlite mixture (4:1). Plants were watered by flooding for 15 min every 2 days. *A. thaliana* knockout and yucca overexpression (OE) lines were described previously (Supplemental information). Estradiol-inducible effector/mCherry lines were created by floral dipping using the XVE:effector-3xMyc construct (Supplemental information). All *A. thaliana* lines were stratified for 3 days at $4^\circ C$ in the dark prior to sowing. Protein expression was induced by estradiol infiltration (20 μM , reporter and ROS burst assays) or spraying (5 μM , *Pseudomonas* infection assays). For auxin treatments, leaves of the appropriate age were infiltrated with 1-NAA (Duchefa) using a needleless syringe, plants were returned

to the growth chamber and incubated for 6 h, and the leaf tissue was then processed as necessary.

Protein production in *N. benthamiana* and colP

For *in vivo* colP assays, *A. tumefaciens* GV3101 (pSoup) carrying the expression constructs were grown overnight in lysogeny broth (LB) supplemented with the appropriate antibiotics at 28°C, centrifuged for 10 min at 1600 × *g*, resuspended in ARM (agrobacterium resuspension medium) buffer (10 mM MES-NaOH pH 5.6, 10 mM MgCl₂, 150 μM acetosyringone) to an OD_{600nm} of 0.2 and incubated for 3 h at room temperature. Cultures carrying the appropriate constructs were then mixed 1:1 and infiltrated into *N. benthamiana* with a needleless syringe. Plants were incubated for 48 h, then frozen in liquid nitrogen, and total proteins were extracted from 300–450 mg of tissue in 2 mL IP buffer (50 mM HEPES pH 7.58, 50 mM NaCl, 10% glycerol, 1 mM EDTA, 0.05% Triton X-100, 1 mM PMSF, and one protease inhibitor tablet [Roche cOmplete EDTA free cat. no. 05056489001]/50 mL). Extracts were cleared by centrifugation for 10 min at 20,000 × *g* 3 times. Proteins were immunoprecipitated by adding 30 μL of α-c-Myc magnetic beads (μMACS Anti-c-Myc Miltenyi Biotec, cat. no. 130-091-284) and incubated for 2 h at 4°C with rotation. Samples were washed 4 times with 300 μL IP buffer, and proteins were eluted by adding 50 μL of 2× SDS loading buffer at 95°C. Next, 10–15 μL of the extracts were analyzed by SDS-PAGE followed by western blotting with α-c-Myc (Sigma-Aldrich, St. Louis, MO, USA) or α-HA (Sigma-Aldrich, St. Louis, MO, USA) antibodies. Experiments were repeated at least three times.

For colP assays of maize tissues, 1-week-old plants were infected with *U. maydis* carrying the appropriate constructs (Supplemental information). Plants were incubated for 7 days, then frozen in liquid nitrogen, and total proteins were extracted from 2–3 g of tissue in 25 mL of IP buffer. Proteins were immunoprecipitated by adding 150 μL of α-c-HA magnetic beads (μMACS Anti-c-Myc Miltenyi Biotec, cat. no. 130-094-255) as described above. Ten to twenty-five microliters of the extracts were analyzed by SDS-PAGE followed by western blotting with α-HA or α-TPL (Eurogentec, Belgium). The latter polyclonal antibodies were developed in rabbit against the peptide CNEQLSKYGDTKSAR, which is conserved across TPL/TPR proteins (Darino et al., 2021). Experiments were repeated two times.

VIGS in *N. benthamiana*

Three-week-old *N. benthamiana* plants were infiltrated with a mixture of *A. tumefaciens* GV3101 (pSoup) strains carrying pTRV1 (OD_{600nm} 0.2), pTRV2-*TPR1* (OD_{600nm} 0.1), and pTRV2-*TPR3* (OD_{600nm} 0.1) in ARM. Control plants were infiltrated with a mixture of strains carrying pTRV1 (OD_{600nm} 0.2) and pTRV2-*GFP* (OD_{600nm} 0.2) (Ratcliff et al., 2001). Plants were then grown for 2–3 weeks before being analyzed. Experiments were repeated three times.

DR5 reporter induction in *N. benthamiana* and *A. thaliana*

Five- to six-week-old *A. thaliana* or 4- to 5-week-old *N. benthamiana* plants were used for the assay. *N. benthamiana* was infiltrated with *A. tumefaciens* carrying the appropriate constructs resuspended in ARM buffer to a final OD_{600nm} of 0.1 and was incubated for 72 h. Leaf disks (4 mm) were cut and floated on water, and GFP fluorescence (485/528 nm) was assessed using a microplate reader (Synergy H1, BioTek). *A. thaliana* leaf disks were incubated overnight prior to fluorescence measurement. At least two *N. benthamiana* or five *A. thaliana* plants per construct/genotype were used in each experiment. Experiments were repeated at least three times.

ROS burst assays in *N. benthamiana*, *A. thaliana*, and maize

A. thaliana and *N. benthamiana* plants were grown as described for the reporter induction assays. Maize plants were 7 days old, and only the first true leaf was used for the assay. Leaf disks (4 mm) were cut and floated on water overnight. For plants expressing pFoMV vectors,

8–9 days after bombardment, leaf disks were cut from areas with positive mCherry fluorescence (indicating viral spread) and floated on water overnight. Water was then removed, and elicitors were added. The flg22-elicitation solution consisted of horseradish peroxidase (HRP; 10 μg/mL, Sigma-Aldrich, cat. no. P6782), L-012 (34 μg/mL Fujifilm WAKO, cat. no. 120-04891), and flg22 (100 nM) in H₂O. Chitin elicitation solution was prepared as follows: 50 mg of chitin (Sigma-Aldrich, cat. no. C9752) was ground with a mortar and pestle in 5 mL of H₂O for 5 min, transferred to a Falcon tube, microwaved for 40 s, sonicated for 5 min, and centrifuged at 1,800 × *g* for 5 min. The supernatant was transferred to a new tube, vortexed for 15 min, and stored at 4°C. Before use, the suspension was diluted 1:1 in H₂O and supplemented with HRP (as described above) and luminol (34 μg/mL Sigma-Aldrich, cat. no. 123072). ROS production was monitored by luminescence over 30–40 min in a microplate reader (Synergy H1, Bio-Tek). At least three *N. benthamiana* or *A. thaliana* plants per construct/genotype were used in each experiment. Experiments were performed at least three times.

Pseudomonas syringae infections in *A. thaliana*

Plants were grown for 1 month under 12 h light/12 h dark conditions at 21°C, sprayed with 5 μM estradiol in 0.01% Silwet, and incubated overnight. *P. syringae* pv. tomato DC3000 was infiltrated into the leaf tissue with a needleless syringe (OD_{600nm} = 0.0002). Plants were covered with a plastic dome and returned to the growth chamber for 2 days. Leaf disks were cut and homogenized in 2-mL tubes containing MgCl₂ and metal beads, and the bacterial load was assessed by plate counts in King's B medium supplemented with rifampicin (50 μg/mL). Plates were incubated at room temperature until colonies were visible. The experiment was repeated three times.

RNA-seq experiments

A. thaliana seedlings were grown vertically for 7 days in 1/2 MS, 2% sucrose plates that contained a nylon mesh (100 μm pore size, SEFAR) under a 16 h/8 h light/dark cycle at 21°C. Protein expression was induced by transferring the nylon mesh with the seedlings onto a new 1/2 MS plate supplemented with β-estradiol (5 μM). Seedlings were then returned to the growth chamber, incubated for 5 or 24 h, and frozen in liquid nitrogen. The experiment was repeated three times. Thirty milligrams of tissue were used for RNA or protein extraction. Expression of β-estradiol-inducible constructs was assessed by western blotting with α-c-Myc antibodies as described earlier. RNA extractions were performed with the RNeasy Plant kit (QIAGEN), and mRNA was isolated from 1 μg of total RNA using the Poly(A) RNA Selection kit (Lexogen). Single-ended, 75-bp libraries were prepared using the Lexogen SENSE kit and sequenced on the Illumina NextSeq 550 platform. Library preparation and sequencing were performed by the VBCF NGS Unit (www.viennabiocenter.org/facilities).

RNA-seq and differential gene expression analysis

Raw RNA-seq data were aligned using STAR v.2.5.1 (Dobin et al., 2013). The average sequencing depth per sample was 33.5 million reads (SD, 3.7 million reads).

Gene expression for all TAIR10 protein-coding genes was calculated using the featureCounts tool from the Subread (v.1.4.6) package (Liao et al., 2014). Expression heatmaps were created from normalized expression data (transcripts per million [TPM]) averaged across three biological replicates using the pheatmap R package with scaling for each gene (scale = "row").

Differential gene expression was assessed with DESeq2 (Love et al., 2014) using the raw count tables generated by featureCounts. Each sample had three replicates.

Statistical analyses

Maize infection assays were analyzed by Fisher's exact test in R as described by [Stirnberg and Djamei \(2016\)](#). All other statistical analyses were performed with GraphPad Prism 8.0. ROS burst data and fluorescence measurements from the DR5 reporter assays were analyzed by Student's *t* test, Tukey's ANOVA, or Bonferroni's two-way ANOVA. *P. syringae* infections (log CFU/cm²) were analyzed by Tukey's ANOVA. Statistical significance was evaluated at the level of $p < 0.05$. For differential gene expression from RNA-seq data, the threshold for calling a gene differentially expressed between two conditions or samples was log₂ fold change > 0.6 and adjusted p value < 0.01.

Data availability

The authors declare that all the data supporting the current findings are available within the paper, [supplemental information](#), source data file, and publicly available databases (for RNA-seq data, GEO: GSE141597).

ACCESSION NUMBERS

The gene accession numbers are as follows: Umnkd1: UMAG_02299; Phnkd1: PHSY_006360; Srnkd1: sr13496; Sgnkd1: EX895_003371; Ssnkd1: SPSC_01711; Mpnkd1: BN887_03254; ZmTPL1: Zm00001d028481; ZmTPL2: Zm00001d040279; ZmTPL3: Zm00001d024523; ZmTPL4: Zm00001d047897; AtTPL: AT1G15750; AtTPR1: AT1G80490; AtTPR2: AT1G04130; AtTPR3: AT5G27030; AtTPR4: AT3G15880; NbTPR1: Niben101Scf19386g00002.1; NbTPR3: Niben101Scf00369g24005.1; MpTPR: Mapoly0051s0078.1; ZmIAA5: Zm00001d039624; AtARF5: AT1G19850; NbARF5: Niben101Scf07465g02002.1; ZmARF2: Zm00001eb045640; ZmARF18: Zm00001eb224680.

SUPPLEMENTAL INFORMATION

Supplemental information is available at [Plant Communications Online](#).

FUNDING

The research leading to these results received funding from the European Research Council under the European Union Seventh Framework Programme ERC-2013-STG grant agreement 335691; the Austrian Science Fund (FWF) P27818-B22, I 3033-B22; the Austrian Academy of Sciences (OEAW); and the Deutsche Forschungsgemeinschaft (DFG, German Research Foundation) under Germany's Excellence Strategy -EXC 2070-390732324.

AUTHOR CONTRIBUTIONS

Conceptualization, F.N., A.D.; funding acquisition, A.D.; investigation: F.N., M.G., M.A.D., A.K., I.S., K.-S.C., M.K.; methodology, F.N., A.D.; project administration, F.N.; resources, F.N., M.G., A.E.K., M.A.D., I.S., J.B., A.D.; supervision, A.D.; writing, F.N., A.D.

ACKNOWLEDGMENTS

We would like to thank the GMI/IMBA/IMP core facilities for excellent technical support, especially the BioOptics and Molecular Biology Services. We thank the Plant Sciences and Next Generation Sequencing Facilities at the Vienna BioCenter Core Facilities GmbH (VBCF). We are grateful to the Jiri Friml and Jürgen Kleine-Vehn laboratories for providing useful *A. thaliana* lines. We thank Mathias Madalinski for peptide synthesis and Dr. J. Matthew Watson for proofreading and valuable feedback on the manuscript. The authors declare no competing interests.

Received: May 18, 2021

Revised: October 21, 2021

Accepted: November 21, 2021

Published: December 17, 2021

REFERENCES

[Alcantara, A., Bosch, J., Fahimeh, N., Hoffmann, G., Gallei, M., Uhse, S., Darino, M.A., Olukayode, T., Reumann, D., Baggaley, L., et al.](#)

(2019). Systematic Y2H screening reveals extensive effector-complex formation. *Front. Plant Sci.* **10**.

[Aliab, S., Bashir, A.G., Kamili, A.N., Bhat, A.A., Mir, Z.A., Bhat, J.A., Tyagi, A., Islam, S.T., Mushtaq, M., Yadava, P., et al.](#) (2018). Pathogenesis-related proteins and peptides as promising tools for engineering plants with multiple stress tolerance. *Microbiol. Res.* **212-213**:29–37.

[Almagro Armenteros, J.J., Tsirigos, K.D., Sønderby, C.K., Petersen, T.N., Winther, O., Brunak, S., von Heijne, G., and Nielsen, H.](#) (2019). SignalP 5.0 improves signal peptide predictions using deep neural networks. *Nat. Biotechnol.* **37**:420–423.

[Altmann, M., Altmann, S., Rodriguez, P.A., Weller, B., Vergara, L.E., Palme, P., Marin-de La Rosa, N., Sauer, M., et al.](#) (2020). Extensive signal integration by the phytohormone protein network. *Nature* **583**:271–276.

[Belkhadir, Y., Yang, L., Hetzel, J., Dangl, J.L., and Chory, J.](#) (2014). The growth–defense pivot: crisis management in plants mediated by LRR-RK surface receptors. *Trends Biochem. Sci.* **39**:447–456.

[Bethany, H., Yao, J., Montgomery, B.L., and Hea, S.Y.](#) (2014). Growth–defense tradeoffs in plants: a balancing act to optimize fitness. *Mol. Plant* **7**:1267–1287.

[Boller, T., and Felix, G.](#) (2009). A renaissance of elicitors: perception of microbe-associated molecular patterns and danger signals by pattern-recognition receptors. *Annu. Rev. Plant Biol.* **60**:379–406.

[Bouton, C., King, R.C., Chen, H.X., Azhakanandam, K., Bieri, S., Hammond-Kosack, K.E., and Kanyuka, K.](#) (2018). Foxtail mosaic virus: a viral vector for protein expression in cereals. *Plant Physiol.* **177**:1352–1367.

[Brachmann, A., Weinzierl, G., Kämper, J., and Kahmann, R.](#) (2001). Identification of genes in the bW/bE regulatory cascade in *Ustilago maydis*. *Mol. Microbiol.* **42**:1047–1063.

[Cai, Q., liang, C., Wang, S., Hou, Y., Gao, L., LIU, L., He, W., Ma, W., Mo, B., and Chen, X.](#) (2019). The disease resistance protein SNC1 represses the biogenesis of microRNAs and phased siRNAs. *Nat. Commun.* **9**:5080.

[Cain, R.J., Hayward, R.D., and Koronakis, V.](#) (2008). Deciphering interplay between *Salmonella* invasion effectors. *PLoS Pathog.* **4**:e1000037.

[Causier, B., Ashworth, M., Guo, W., and Davies, B.](#) (2012). The toplless interactome: a framework for gene repression in *Arabidopsis*. *Plant Physiol.* **158**:423–438.

[Chen, Z., Agnew, J.L., Cohen, J.D., He, P., Shan, L., Sheen, J., and Kunkel, B.N.](#) (2007). *Pseudomonas syringae* type III effector AvrRpt2 alters *Arabidopsis thaliana* auxin physiology. *PNAS* **104**:20131–20136.

[Consortium, A.I.M.](#) (2011). Evidence for network evolution in an *Arabidopsis* interactome map. *Science* **333**:601–607.

[Cui, F., Wu, S., Sun, W., Coaker, G., Kunkel, B., He, P., and Shan, L.](#) (2013). The *Pseudomonas syringae* type III effector AvrRpt2 promotes pathogen virulence via stimulating *Arabidopsis* auxin/indole acetic acid protein turnover. *Plant Physiol.* **162**:1018–1029.

[Dangl, J.L., and Jones, J.D.G.](#) (2006). The plant immune system. *Nature* **444**:323–329.

[Darino, M., Chia, K.S., Marques, J., Aleksza, D., Soto-Jimenez, L.M., Saado, I., Uhse, S., Borg, M., Betz, R., Bindics, J., et al.](#) (2021). *Ustilago maydis* effector Jsi1 interacts with Topless corepressor, hijacking plant jasmonate/ethylene signaling. *New Phytol.* **229**:3393–3407.

[Ding, X., Cao, Y., Huang, L., Zhao, J., Xu, C., Li, X., and Wang, S.](#) (2008). Activation of the indole-3-acetic acid-amido synthetase

- GH3-8 suppresses expansin expression and promotes salicylate- and jasmonate-independent basal immunity in rice. *Plant Cell* **20**:228–240.
- Djamei, A., Schipper, K., Rabe, F., et al.** (2011). Metabolic priming by a secreted fungal effector. *Nature* **478**:395–398.
- Dobin, A., Davis, C.A., Schlesinger, F., Drenkow, J., Zaleski, C., Jha, S., Batut, P., Chaisson, M., and Gingeras, T.R.** (2013). STAR: ultrafast universal RNA-seq aligner. *Bioinformatics* **29**:15–21.
- Dodds, P.N., and Rathjen, J.P.** (2010). Plant immunity: towards an integrated view of plant–pathogen interactions. *Nat. Rev. Genet.* **11**:539–548.
- Doehlemann, G., Reissmann, S., Assmann, D., Fleckenstein, M., and Kahmann, R.** (2011). Two linked genes encoding a secreted effector and a membrane protein are essential for *Ustilago maydis*-induced tumour formation. *Mol. Microbiol.* **81**:751–766.
- Doehlemann, G., van der Linde, K., Assmann, D., Schwambach, D., Hof, A., Mohanty, A., Jackson, D., and Kahmann, R.** (2009). Pep1, a secreted effector protein of *Ustilago maydis*, is required for successful invasion of plant cells. *PLoS Pathog.* **5**:e1000290.
- Doehlemann, G., Wahl, R., Horst, R.J., Voll, L.M., Usadel, B., Poree, F., Stitt, M., Pons-Kuhnemann, J., Sonnewald, U., Kahmann, R., et al.** (2008). Reprogramming a maize plant: transcriptional and metabolic changes induced by the fungal biotroph *Ustilago maydis*. *Plant J.* **56**:181–195.
- Evangelisti, E., Govetto, B., Minet-Kebdani, N., Kuhn, M.L., Attard, A., Ponchet, M., Panabieres, F., and Gourgues, M.** (2013). The *Phytophthora parasitica* RXLR effector penetration-specific effector 1 favours *Arabidopsis thaliana* infection by interfering with auxin physiology. *New Phytol.* **199**:476–489.
- Fernandez-Bautista, N., Domínguez-Núñez, J.A., Castellano Moreno, M.M., and Berrocal-Lobo, M.** (2016). Plant tissue trypan blue staining during phytopathogen infection. *Bioprotocols* **6**:e2078.
- Gawehns, F.K.K.** (2014). Function and targets of fusarium oxysporum effectors. Dissertation.
- Gookin, T.E., and Assmann, S.M.** (2014). Significant reduction of BiFC non-specific assembly facilitates in planta assessment of heterotrimeric G-protein interactors. *Plant J.* **80**:553–567.
- Hentrich, M., Böttcher, C., Düchting, P., Cheng, Y., zhao, Y., Berkowitz, O., Masle, J., Medina, J., and Pollmann, S.** (2013). The jasmonic acid signaling pathway is linked to auxin homeostasis through the modulation of YUCCA8 and YUCCA9 gene expression. *Plant J.* **74**:626–637.
- Hiratsu, K., Matsui, K., Koyama, T., and Ohme-Takagi, M.** (2003). Dominant repression of target genes by chimeric repressors that include the EAR motif, a repression domain, in *Arabidopsis*. *Plant J.* **34**:733–739.
- Jiang, S., Yao, J., Ma, K., Zhou, H., Song, J., He, S.H., and Ma, W.** (2013). Bacterial effector activates jasmonate signaling by directly targeting JAZ transcriptional repressors. *PLoS Biol.* **9**:e1003715.
- Jones, K., Kim, D.W., Park, J.S., and Khang, C.H.** (2016). Live-cell fluorescence imaging to investigate the dynamics of plant cell death during infection by the rice blast fungus *Magnaporthe oryzae*. *BMC Plant Biol.* **16**:69.
- Kämper, J.** (2004). A PCR-based system for highly efficient generation of gene replacement mutants in *Ustilago maydis*. *Mol. Genet. Genomics* **271**:103–110.
- Kämper, J., Kahmann, R., Bolker, M., Ma, L.J., Brefort, T., Saville, B.J., Banuett, F., Kronstad, J.W., Gold, S.E., Muller, O., et al.** (2006). Insights from the genome of the biotrophic fungal plant pathogen *Ustilago maydis*. *Nature* **444**:97–101.
- Katzen, F.** (2007). Gateway® recombinational cloning: a biological operating system. *Expert Opin. Drug Discov.* **2**:571–589.
- Ke, J., Ma, H., Gu, X., Thelen, A., Brunzelle, J.S., Li, J., Xu, H.E., and Melcher, K.** (2015). Structural basis for recognition of diverse transcriptional repressors by the TOPLESS family of corepressors. *Sci. Adv.* **1**:e1500107.
- Lampropoulos, A., Sutikovic, Z., Wenzl, C., Maegerle, I., Lohmann, J.U., and Forner, J.** (2013). GreenGate - a novel, versatile, and efficient cloning system for plant transgenesis. *PLoS One* **8**:e83043.
- Lanver, D., Muller, A.N., Happel, P., Schweizer, G., Haas, F.B., Franitza, M., Pellegrin, C., Reissmann, S., Altmüller, J., Rensing, S.A., et al.** (2018). The biotrophic development of *Ustilago maydis* studied by RNA-seq analysis. *Plant Cell* **30**:300–323.
- Liao, Y., Smyth, G.K., and Shi, W.** (2014). featureCounts: an efficient general purpose program for assigning sequence reads to genomic features. *Bioinformatics* **30**:923–930.
- Lin, F., Jiang, L., Liu, Y., Lv, Y., Dai, H., and Zhao, H.** (2014). Genome-wide identification of housekeeping genes in maize. *Plant Mol. Biol.* **86**:543–554.
- Livak, K.J., and Schmittgen, D.** (2001). Analysis of relative gene expression data using real time quantitative PCR and the 2- $\Delta\Delta CT$ method. *Methods* **25**:402–408.
- Lo Presti, L., Zechmann, B., Kümlehn, J., Liang, L., Lanver, D., Tanaka, S., Bock, R., and Kahmann, R.** (2017). An assay for entry of secreted fungal effectors into plant cells. *New Phytol.* **213**:956–964.
- Long, J.A., Ohno, C., Smith, Z.R., and Meyerowitz, E.M.** (2006). Topless regulates apical embryonic fate in *Arabidopsis*. *Science* **312**:1520–1523.
- Loubradou, G., Brachmann, A., Feldbrugge, M., and Kahmann, R.** (2001). A homologue of the transcriptional repressor Ssn6p antagonizes cAMP signalling in *Ustilago maydis*. *Mol. Microbiol.* **40**:719–730.
- Love, M.I., Huber, W., and Anders, S.** (2014). Moderated estimation of fold change and dispersion for RNA-seq data with DESeq2. *Genome Biol.* **15**:550.
- Lu, H., Rate, D.N., Song, J.T., and Greenberg, J.T.** (2003). ACD6, a novel ankyrin protein, is a regulator and an effector of salicylic acid signaling in the *Arabidopsis* defense response. *Plant Cell* **15**:2408–2420.
- Lynch, T.J., Erickson, J., Miller, D.R., and Finkelstein, R.R.** (2017). ABI5-binding proteins (ABFs) alter transcription of ABA-induced genes via a variety of interactions with chromatin modifiers. *Plant Mol. Biol.* **93**:403–418.
- Magori, S., and Citovsky, V.** (2011). *Agrobacterium* counteracts host-induced degradation of its effector F-box protein. *Sci. Signal.* **4**:ra69.
- Martin-Arevalillo, R., Nanao, M.H., Larrieu, A., Vinos-Poyo, T., Mast, D., Galvan-Ampudia, C., Brunoud, G., Vernoux, T., Dumas, R., and Parcy, F.** (2017). Structure of the *Arabidopsis* TOPLESS corepressor provides insight into the evolution of transcriptional repression. *Proc. Natl. Acad. Sci. U S A* **114**:8107–8112.
- Mcclerklin, S.A., Lee, S.G., Harper, C.P., Nwumeh, R., Jez, J.M., and Kunkel, B.N.** (2018). Indole-3-acetaldehyde dehydrogenase-dependent auxin synthesis contributes to virulence of *Pseudomonas syringae* strain DC3000. *PLoS Biol.* **14**:e1006811.
- Mockaitis, K., and Estelle, M.** (2008). Auxin receptors and plant development: a new signaling paradigm. *Annu. Rev. Cell Dev. Biol.* **24**:55–80.
- Mudgett, M.B., Chesnokova, O., Dahlbeck, D., Clark, E.T., Rossier, O., Bonas, U., and Staskawicz, B.J.** (2000). Molecular signals required for type III secretion and translocation of the *Xanthomonas campestris*

- AvrBs2 protein to pepper plants. *Proc. Natl. Acad. Sci. U S A* **97**:13324–13329.
- Mutka, A.M., Fawley, S., Tsao, T., and Kunkel, B.N. (2013). Auxin promotes susceptibility to *Pseudomonas syringae* via a mechanism independent of suppression of salicylic acid-mediated defenses. *Plant J.* **74**:746–754.
- Navarrete, F., Grujic, N., Stirnberg, A., Saado, I., Aleksza, D., Gallei, M., Adi, H., Alcantara, A., Khan, M., Bindics, J., et al. (2021). The Pleiades are a cluster of fungal effectors that inhibit host defenses. *PLoS Pathog.* **17**:e1009641.
- Navarro, L., Dunoyer, P., Jay, F., Arnold, B., Dharmasiri, N., Estelle, M., Voinnet, O., and Jones, J.D.G. (2006). A plant miRNA contributes to antibacterial resistance by repressing auxin signaling. *Science* **312**:436–439.
- Navarro, L., Dunoyer, P., Zipfel, C., Rowland, O., Keller, I., Robatzek, S., Boller, T., and Jones, J.D.G. (2004). The transcriptional innate immune response to flg22. Interplay and overlap with Avr gene-dependent defense responses and bacterial pathogenesis. *Plant Physiol.* **135**:1113–1128.
- Ngou, B.P.M., Ahn, H.-K., Ding, P., and Jones, J.D.G. (2021). Mutual potentiation of plant immunity by cell-surface and intracellular receptors. *Nature* **592**:110–115.
- Niu, D., Lin, X., Kong, X., Qu, G., Cai, B., Lee, J., and Jin, J.B. (2019). SIZ1-Mediated SUMOylation of TPR1 suppresses plant immunity in *Arabidopsis*. *Mol. Plant* **12**:215–228.
- Oh, E., Zhu, J., Ryu, H., Hwang, I., and Wang, Z. (2014). TOPLESS mediates brassinosteroid-induced transcriptional repression through interaction with BZR1. *Nat. Commun.* **5**:4140.
- Park, C., Chen, S., Shirsekar, G., Zhou, B., Hyun Khang, C., Songkumarn, P., Afzal, A.J., Ning, Y., Wang, R., Bellizzi, M., et al. (2012). The Magnaporthe oryzae effector AvrPiz-t targets the RING E3 ubiquitin ligase APIP6 to suppress pathogen-associated molecular pattern-triggered immunity in rice. *Plant Cell* **24**:4748–4762.
- Pauwels, L., Fernandez Barbero, G., Geerinck, J., Tilleman, S., Grunewald, W., Cuellar Perez, A., Chico, J.M., van den Bossche, R., Sewell, J., Gil, E., et al. (2010). Ninja connects the co-repressor topless to jasmonate signalling. *Nature* **464**:788–793.
- Petre, B., Saunders, D.G., Sklenar, J., Lorrain, C., Win, J., Duplessis, S., and Kamoun, S. (2015). Candidate effector proteins of the rust pathogen *Melampsora larici-populina* target diverse plant cell compartments. *Mol. Plant Microbe Interact.* **28**:689–700.
- Ratcliff, F., Martin-Hernandez, A.M., and Baulcombe, D.C. (2001). Technical advance. *Tobacco rattle virus* as a vector for analysis of gene function by silencing. *Plant J.* **25**:237–245.
- Redkar, A., Hoser, R., Schilling, L., Zechmann, B., krzymowska, M., Walbot, V., and Doehlemann, G. (2015). A secreted effector protein of *Ustilago maydis* guides maize leaf cells to form tumors. *Plant Cell* **27**:1332–1351.
- Reinecke, G., Heinze, B., Schirawski, J., Buettner, H., Kahmann, R., and Basse, C.W. (2008). Indol-3-acetic acid biosynthesis in the smut fungus *Ustilago maydis* and its relevance for increased IAA levels in infected tissue and host tumour formation. *Mol. Plant Pathol.* **9**:339–355.
- Robert-Seilaniantz, A., Grant, M., and Jones, J.D. (2011). Hormone crosstalk in plant disease and defense: more than just jasmonate-salicylate antagonism. *Annu. Rev. Phytopathol.* **49**:317–343.
- Sambrook, J., Russell, D.W., and Sambrook, J. (2006). *The Condensed Protocols from Molecular Cloning: A Laboratory Manual* (Cold Spring Harbor: Cold Spring Harbor Laboratory Press).
- Schindelin, J., Arganda-Carreras, I., Frise, E., Kaynig, V., Longair, M., Pietzsch, T., Preibisch, S., Rueden, C., Saalfeld, S., Schmid, B., et al. (2012). Fiji: an open-source platform for biological-image analysis. *Nat. Methods* **9**:676–682.
- Schirawski, J., Mannhaupt, G., Munch, K., Brefort, T., Schipper, K., Doehlemann, G., di Stasio, M., Rosset, N., Mendoza-Mendoza, A., Pester, D., et al. (2010). Pathogenicity determinants in smut fungi revealed by genome comparison. *Science* **330**:1546–1548.
- Shi, X., Long, Y., He, F., Zhang, C., Wang, R., Zhang, T., Wu, W., Hao, Z., Wang, Y.L., Wang, G., et al. (2018). The fungal pathogen *Magnaporthe oryzae* suppresses innate immunity by modulating a host potassium channel. *PLoS Pathog.* **14**:e1006878.
- Stirnberg, A., and Djamei, A. (2016). Characterization of ApB73, a virulence factor important for colonization of *Zea mays* by the smut *Ustilago maydis*. *Mol. Plant Pathol.* **17**:1467–1479.
- Suzuki, S., He, Y., and Oyaizu, H. (2003). Indole-3-acetic acid production in *Pseudomonas fluorescens* HP72 and its association with suppression of creeping bentgrass brown patch. *Curr. Microbiol.* **47**:138–143.
- Szemenyei, H., Hannon, M., and Long, J.A. (2008). Topless mediates auxin-dependent transcriptional repression during *Arabidopsis* embryogenesis. *Science* **319**:1384–1386.
- Tanaka, S., Brefort, T., Neidig, N., Djamei, A., Kahnt, J., Vermerris, W., Koenig, S., Feussner, K., Feussner, I., and Kahmann, R. (2014). A secreted *Ustilago maydis* effector promotes virulence by targeting anthocyanin biosynthesis in maize. *Elife* **3**:e01355.
- Tanaka, S., Djamei, A., Lo Presti, L., Schipper, K., Winterberg, S., Amati, S., Becker, D., Buchner, H., Kümlehn, J., Reissmann, S., et al. (2015). Experimental approaches to investigate effector translocation into host cells in the *Ustilago maydis*/maize pathosystem. *Eur. J. Cell Biol.* **94**:349–358.
- Tateda, C., Zhang, Z., Shrestha, J., Jelenska, J., Chinchilla, D., and Greenberg, J.T. (2014). Salicylic acid regulates *Arabidopsis* microbial pattern receptor kinase levels and signaling. *Plant Cell* **26**:4171–4187.
- Tsuda, K., Sato, M., Glazebrook, J., Cohen, J.D., and Katagiri, F. (2008). Interplay between MAMP-triggered and SA-mediated defense responses. *Plant J.* **53**:763–775.
- Turian, G., and Hamilton, R.H. (1960). Chemical detection of 3-indolylacetic acid in *Ustilago zeae* tumors. *Biochim. Biophys. Acta* **41**:148–150.
- Tzfira, T., Vaidya, M., and Citovsky, V. (2004). Involvement of targeted proteolysis in plant genetic transformation by *Agrobacterium*. *Nature* **431**:87–92.
- Wang, Y., Wang, Y., Tan, Q., Gao, Y.N., Li, Y., and Bao, D.P. (2017). Comparison and validation of putative pathogenicity-related genes identified by T-DNA insertional mutagenesis and microarray expression profiling in *Magnaporthe oryzae*. *Biomed. Res. Int.* **2017**:7198614.
- Weigel, R.R., Bäuscher, C., Pfitzner, A.J.P., and Pfitzner, U.M. (2001). NIMIN-1, NIMIN-2 and NIMIN-3, members of a novel family of proteins from *Arabidopsis* that interact with NPR1/NIM1, a key regulator of systemic acquired resistance in plants. *Plant Mol. Biol.* **46**:143–160.
- Xin, X., Kvitko, B., and HE, S.Y. (2018). *Pseudomonas syringae*: what it takes to be a pathogen. *Nat. Rev. Microbiol.* **16**:316–328.
- Xing, H., Pudake, R.N., Guo, G., Xing, G., Hu, Z., Zhang, Y., Sun, Q., and Ni, Z. (2011). Genome-wide identification and expression profiling of auxin response factor (ARF) gene family in maize. *BMC Genomics* **12**:178.
- Yamada, T. (1993). The role of auxin in plant-disease development. *Annu. Rev. Phytopathol.* **31**:253–273.

- Yuan, M., Jiang, Z., Bi, G., nomura, K., Liu, M., wang, Y., Cai, B., Zhou, J.M., He, S.Y., and Xin, X.F.** (2021). Pattern-recognition receptors are required for NLR-mediated plant immunity. *Nature* **592**:105–109.
- Zhang, Z.Q., Guo, J.J., Zhao, Y.F., and Chen, J.T.** (2019). Identification and characterization of maize ACD6-like gene reveal ZmACD6 as the maize orthologue conferring resistance to *Ustilago maydis*. *Plant Signal. Behav.* **14**:e1651604.
- Zhao, Y., Christensen, S.K., Fankhauser, C., Cashman, J.R., Cohen, J.D., Weigel, D., and chory, J.** (2001). A role for flavin monooxygenase-like enzymes in auxin biosynthesis. *Science* **291**:306–309.
- Zhu, Z., Xu, F., Zhang, Y., Cheng, Y.T., Wiermer, M., Li, X., and Zhang, Y.** (2010). Arabidopsis resistance protein SNC1 activates immune responses through association with a transcriptional corepressor. *Proc. Natl. Acad. Sci. U S A* **107**:13960–13965.
- Ziemann, S., van der Linde, K., Lahrmann, U., Acar, B., Kaschani, F., Colby, T., Kaiser, M., Ding, Y.Z., Schmelz, E., Huffaker, A., et al.** (2018). An apoplastic peptide activates salicylic acid signalling in maize. *Nat. Plants* **4**:172–180.
- Ding, Y.L., Sun, T.J., Ao, K., et al.** (2018). Opposite roles of salicylic acid receptors NPR1 and NPR3/NPR4 in transcriptional regulation of plant immunity. *Cell* **173**:1454.